



Prompt Λ_c^+ production in $p\text{Pb}$ collisions at $\sqrt{s_{\text{NN}}} = 5.02 \text{ TeV}$

LHCb collaboration[†]

Abstract

The prompt production of Λ_c^+ baryons is studied in proton-lead collisions collected with the LHCb detector at the LHC. The data sample corresponds to an integrated luminosity of 1.58 nb^{-1} recorded at a nucleon-nucleon centre-of-mass energy of $\sqrt{s_{\text{NN}}} = 5.02 \text{ TeV}$. Measurements of the differential cross-section and the forward-backward production ratio are reported for Λ_c^+ baryons with transverse momenta in the range $2 < p_{\text{T}} < 10 \text{ GeV}/c$ and rapidities in the ranges $1.5 < y^* < 4.0$ and $-4.5 < y^* < -2.5$ in the nucleon-nucleon centre-of-mass system. The ratio of cross-sections of Λ_c^+ baryons and D^0 mesons is also reported. The results are compared with next-to-leading order calculations that use nuclear parton distribution functions.

Published in JHEP 02 (2019) 102

© 2019 CERN for the benefit of the LHCb collaboration. CC-BY-4.0.

[†]Authors are listed at the end of this paper.

1 Introduction

The ultimate goal of relativistic heavy-ion collision experiments at the SPS, RHIC and the LHC accelerators is to learn about the properties of a new state of matter, the quark-gluon plasma (QGP). The QGP consists of deconfined quarks and gluons and it is generally accepted that such a hot and dense state of matter can be produced in high-energy heavy-ion collisions [1]. Heavy quarks are particularly important probes of the properties of the QGP. According to theoretical models, heavy quarks are created in pairs in the early stage of the space-time evolution of heavy-ion collisions, and undergo rescattering or energy loss in the QGP. Measurements of heavy-flavour production can shed light on the transport properties of the medium and the heavy-quark energy-loss mechanisms. Multiple experimental measurements of D -meson production in heavy-ion collisions at RHIC [2] and the LHC [3] already show clear signs of strong interactions between charm quarks and the medium in these collisions. However, heavy quarks can be affected by both hot and cold nuclear matter, since cold nuclear matter effects are also present in nucleus-nucleus interactions. Possible cold nuclear matter effects that affect heavy-flavour production in heavy-ion collisions include: (a) the modification of the parton distribution function in bound nucleons in the initial state, namely the nuclear PDF (nPDF) effects [4, 5]; (b) initial-state radiation or energy loss due to soft collisions [6–8]; and (c) final-state hadronic rescatterings and absorption [9]. To further study heavy-quark energy loss or collective phenomena in QGP, the cold nuclear matter effects must be quantitatively disentangled from hot nuclear matter effects.

LHCb measurements can play an important role in understanding cold nuclear matter effects, thanks to LHCb detector’s outstanding capability in heavy-flavour measurements. The precise tracking system allows the separation of “prompt” charm hadrons, which are directly produced in p Pb collisions, from “nonprompt” charm hadrons coming from decays of b hadrons. The excellent particle identification capabilities of the LHCb detector allow measurements of various species of charmed hadrons. Finally, prompt open-charm hadrons can be measured down to low transverse momentum (p_T) at forward rapidity (y) owing to the LHCb’s geometric coverage. These measurements provide sensitive probes of the nPDF in the low parton fractional longitudinal momentum (x) region down to $x \approx 10^{-6}$ – 10^{-5} , where the nPDF is largely unconstrained by experimental data.

Prompt D^0 meson production has been measured by the LHCb collaboration in p Pb collisions at $\sqrt{s_{NN}} = 5.02$ TeV with data recorded in 2013 [10]. In the present study, the production of the charmed baryon Λ_c^+ is measured with the same 2013 data sample.¹ The forward-backward asymmetry is measured using prompt Λ_c^+ candidates, in order to study cold nuclear matter effects. In addition, the baryon-to-meson cross-section ratios are measured in order to probe the charm-hadron formation mechanism [11, 12] using D^0 production cross-sections measured by the LHCb collaboration in Ref. [10]. Measurements of the baryon-to-meson cross-section ratios for light and strange hadrons have shown significant baryon enhancement at intermediate p_T in the most central heavy-ion collisions [13, 14]. This enhancement can be explained by coalescence models [11, 15–18], which assume that all hadrons are formed through recombination of partons during hadronisation. Recently, the STAR experiment has measured the production of Λ_c^+ baryons in AuAu collisions at $\sqrt{s_{NN}} = 200$ GeV [19]. These measurements show a

¹ Charge conjugation states and processes are implied throughout the paper.

significant enhancement in the Λ_c^+ to D^0 yield ratio for p_T from 3 to 6 GeV/ c . A similar enhancement in PbPb collisions is also observed by the ALICE experiment [20]. The measurement of Λ_c^+ production in p Pb collisions provides complementary information to help understand the implications of the STAR and ALICE observations. In addition, the ALICE collaboration has recently measured Λ_c^+ production in p Pb collisions at $\sqrt{s_{NN}} = 5.02$ TeV for $2 < p_T < 12$ GeV/ c and $-0.96 < y < 0.04$, and in pp collisions at $\sqrt{s} = 7$ TeV for $1 < p_T < 8$ GeV/ c and $-0.5 < y < 0.5$ [21]. The LHCb collaboration has also published results on the production cross-section of prompt Λ_c^+ baryons in pp collisions at $\sqrt{s} = 7$ TeV [22].

2 Detector and data

The LHCb detector [23, 24] is a single-arm forward spectrometer covering the pseudorapidity range $2 < \eta < 5$, designed for the study of particles containing b or c quarks. The detector includes a high-precision tracking system consisting of a silicon-strip vertex detector surrounding the pp interaction region (VELO), a large-area silicon-strip detector located upstream of a dipole magnet with a bending power of about 4 Tm, and three stations of silicon-strip detectors and straw drift tubes placed downstream of the magnet. The tracking system provides a measurement of the momentum of charged particles with a relative uncertainty that varies from 0.5% at low momentum to 1.0% at 200 GeV/ c . The minimum distance of a track to a primary vertex (PV), the impact parameter, is measured with a resolution of $(15 + 29/p_T)$ μm in GeV/ c . Different types of charged hadrons are distinguished using information from two ring-imaging Cherenkov detectors. The average efficiency for kaon identification for momenta between 2 and 100 GeV/ c is about 95%, with a corresponding average pion misidentification rate around 5%. Photons, electrons and hadrons are identified by a calorimeter system consisting of scintillating-pad and preshower detectors, an electromagnetic calorimeter and a hadronic calorimeter. Muons are identified by a system composed of alternating layers of iron and multiwire proportional chambers. The online event selection is performed by a trigger, which consists of a hardware stage, based on information from the calorimeter and muon systems, followed by a software stage, which applies a full event reconstruction.

This analysis uses the data sample of p Pb collisions at $\sqrt{s_{NN}} = 5.02$ TeV taken with the LHCb detector in 2013, with a proton beam energy of 4 TeV and lead beam energy of 1.58 TeV per nucleon in the laboratory frame. Since the LHCb detector covers only one direction of the full rapidity acceptance, two distinctive beam configurations were used. In the ‘forward’ (‘backward’) configuration, the proton (lead) beam travels from the VELO detector to the muon chambers. The rapidity y in the laboratory rest frame is shifted to $y^* = y - 0.4645$ in the proton-nucleon rest frame. Here, y^* is the rapidity of the Λ_c^+ baryon defined in the centre-of-mass system of the colliding nucleons, and it is defined with respect to a polar axis in the direction of the proton beam. During data taking, the hardware trigger operated in a ‘pass-through’ mode that accepted all bunch crossings, regardless of the inputs from the calorimeter and muon systems. The software trigger accepted all events with a minimum activity in the VELO. The integrated luminosity of the sample was determined in Ref. [25], and is $1.06 \pm 0.02 \text{ nb}^{-1}$ ($0.52 \pm 0.01 \text{ nb}^{-1}$) for the forward (backward) collisions, respectively. Due to the low beam intensity, multiple interactions in the bunch crossings are very rare, and only a single PV is reconstructed

for each event.

Simulated $p\text{Pb}$ collisions at 5 TeV at both configurations with full event reconstruction are used in the analysis to evaluate the detector efficiency. In the simulation, Λ_c^+ baryons are generated with PYTHIA [26] and embedded into minimum-bias $p\text{Pb}$ collisions from the EPOS event generator [27], which is tuned with LHC data [28]. Decays of hadronic particles are described by EVTGEN [29], in which final-state radiation is generated using PHOTOS [30]. The interaction of the generated particles with the detector, and its response, are implemented using the GEANT4 toolkit [31, 32] as described in Ref. [33].

3 Cross-section determination

The differential production cross-section of Λ_c^+ baryons is measured in bins of the Λ_c^+ transverse momentum and rapidity in the kinematic range $2 < p_{\text{T}} < 10 \text{ GeV}/c$ with $1.5 < y^* < 4.0$ for the forward sample and $-4.5 < y^* < -2.5$ for the backward sample. The double-differential cross-section is obtained using

$$\frac{d^2\sigma}{dy^*dp_{\text{T}}} = \frac{N(\Lambda_c^+ \rightarrow pK^-\pi^+)}{\mathcal{L} \times \varepsilon_{\text{tot}} \times \mathcal{B}(\Lambda_c^+ \rightarrow pK^-\pi^+) \times \Delta y^* \times \Delta p_{\text{T}}}, \quad (1)$$

where $N(\Lambda_c^+ \rightarrow pK^-\pi^+)$ is the prompt Λ_c^+ signal yield reconstructed in the $\Lambda_c^+ \rightarrow pK^-\pi^+$ decay channel in each (p_{T}, y^*) bin, \mathcal{L} is the integrated luminosity, ε_{tot} is the total efficiency determined in each (p_{T}, y^*) bin, $\mathcal{B}(\Lambda_c^+ \rightarrow pK^-\pi^+) = (6.35 \pm 0.33)\%$ is the branching fraction of the decay $\Lambda_c^+ \rightarrow pK^-\pi^+$ [34]. The signal yields and efficiencies are determined independently for each p_{T} and y^* bin of width $\Delta p_{\text{T}} = 1 \text{ GeV}/c$ and $\Delta y^* = 0.5$. The total cross-section is calculated by integrating the double differential cross-section over a given kinematic range.

The forward-backward ratio R_{FB} measures the Λ_c^+ production asymmetry in the forward and backward rapidity regions. It is defined as

$$R_{\text{FB}}(y^*, p_{\text{T}}) \equiv \frac{d^2\sigma(y^*, p_{\text{T}}; y^* > 0)/dy^*dp_{\text{T}}}{d^2\sigma(y^*, p_{\text{T}}; y^* < 0)/dy^*dp_{\text{T}}}, \quad (2)$$

where $\sigma(y^*, p_{\text{T}}; y^* > 0)$ and $\sigma(y^*, p_{\text{T}}; y^* < 0)$ correspond to the cross-sections of the forward and backward rapidity regions symmetric around $y^* = 0$, respectively. The R_{FB} ratio is measured in the common rapidity region of the forward and backward data $2.5 < |y^*| < 4.0$.

The baryon-to-meson cross-section ratio $R_{\Lambda_c^+/D^0} \equiv \sigma(\Lambda_c^+)/\sigma(D^0)$ is calculated as the ratio of Λ_c^+ and D^0 production cross-sections

$$R_{\Lambda_c^+/D^0}(y^*, p_{\text{T}}) = \frac{d^2\sigma_{\Lambda_c^+}(y^*, p_{\text{T}})/dy^*dp_{\text{T}}}{d^2\sigma_{D^0}(y^*, p_{\text{T}})/dy^*dp_{\text{T}}}, \quad (3)$$

where $\sigma_{\Lambda_c^+}$ and σ_{D^0} are cross-sections of Λ_c^+ and D^0 hadrons in $p\text{Pb}$ collisions at $\sqrt{s_{\text{NN}}} = 5.02 \text{ TeV}$, respectively. The D^0 production cross-section in the kinematic region $0 < p_{\text{T}} < 10 \text{ GeV}/c$ with $1.5 < y^* < 4.0$ for the forward sample and $-5.0 < y^* < -2.5$ for the backward sample has been measured by the LHCb collaboration and is documented in Ref. [10]. As the D^0 meson sample is significantly larger and has a better signal purity than that of Λ_c^+ baryons, the D^0 production cross-section can be measured in a wider rapidity range in the backward sample.

3.1 Event selection

Proton, kaon and pion candidates are selected with particle identification (PID) [35] criteria, and are required to be inconsistent with originating from any PV. Random combinations of charged particles form a larger background in the backward sample than in the forward sample, due to a larger number of tracks per event. Each possible combination of the selected decay products undergoes further selection to reject false Λ_c^+ candidates from such random combinations. The requirements applied to select a reconstructed Λ_c^+ candidate include: (a) its reconstructed invariant mass is in the range $[M_{\Lambda_c^+} - 75 \text{ MeV}/c^2, M_{\Lambda_c^+} + 75 \text{ MeV}/c^2]$, which corresponds to around 25 times the mass resolution around the measured Λ_c^+ mass $M_{\Lambda_c^+} = 2288.7 \text{ MeV}/c^2$, which is $2.2 \text{ MeV}/c^2$ larger than the known Λ_c^+ mass $2286.46 \text{ MeV}/c^2$ [34]; (b) the angle between the reconstructed Λ_c^+ momentum and the vector pointing from the PV to the decay vertex is close to zero. (c) the proper decay time of the Λ_c^+ candidate is in the range $[0.1, 1.2] \text{ ps}$; (d) the p , K^- and π^+ candidates form a good-quality vertex; and (e) the decay vertex is significantly separated from the PV. After the selection, about 1% of the events are found to contain multiple candidates. All candidates are kept. Few Λ_c^+ baryons are observed with $p_T < 2 \text{ GeV}/c$ due to low efficiencies, while the combinatorial background is large. Therefore the measurement is restricted to $p_T > 2 \text{ GeV}/c$.

3.2 Prompt Λ_c^+ yield and efficiencies

The Λ_c^+ signal includes both prompt and nonprompt components. The nonprompt Λ_c^+ candidates originate from b -hadron decays, denoted Λ_c^+ -from- b hereafter. The number of prompt Λ_c^+ candidates, $N(\Lambda_c^+ \rightarrow pK^-\pi^+)$, in Eq. 1 is estimated following the strategy developed in previous LHCb charm analyses in pp collisions at $\sqrt{s} = 7 \text{ TeV}$ [22] and in $p\text{Pb}$ collisions at $\sqrt{s_{\text{NN}}} = 5.02 \text{ TeV}$ [10]. The invariant-mass distribution, $m(pK^-\pi^+)$, is first fitted to determine the yield of inclusive Λ_c^+ candidates in the sample. The prompt Λ_c^+ fraction is then determined from a fit to the distribution of the χ^2 of the impact parameter of the Λ_c^+ candidates ($\chi_{\text{IP}}^2(\Lambda_c^+)$), which is defined as the difference in the vertex fit χ^2 of a given PV when it is reconstructed with and without the Λ_c^+ candidate.

Figure 1 shows the fit result of an extended unbinned maximum-likelihood fit to the $m(pK^-\pi^+)$ distribution of the full dataset, which contains 11.6×10^3 (4.0×10^3) Λ_c^+ baryons for the forward (backward) sample. A Gaussian function is used to describe the shape of the Λ_c^+ signal, while the combinatorial background is modelled by a linear function. Although Fig. 1 corresponds to the full dataset, independent fits are performed in each (p_T, y^*) bin. The width and peak position of the Gaussian function depends on the kinematics of the Λ_c^+ baryons, due to the imperfect detector alignment, and both are therefore left as free parameters in the fits. The peak position varies between 2284 and 2294 MeV/c^2 , and the width is found to be between 4 and 10 MeV/c^2 .

Unlike prompt Λ_c^+ baryons, which originate from the PV, Λ_c^+ -from- b baryons are created away from the PV due to the relatively long lifetime of b hadrons. Decay products of Λ_c^+ -from- b candidates tend to have larger impact parameter with respect to the PV and a larger χ_{IP}^2 , compared to the prompt Λ_c^+ candidates. Consequently, the fraction of prompt Λ_c^+ baryons is determined from a fit to the distribution of $\log_{10} \chi_{\text{IP}}^2(\Lambda_c^+)$ using the different χ_{IP}^2 distributions describing the prompt Λ_c^+ , the Λ_c^+ -from- b , and the combinatorial background contributions.

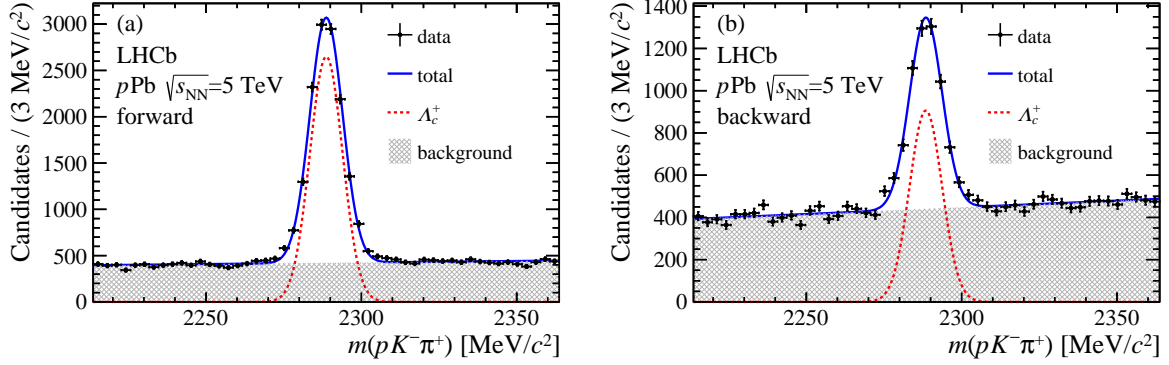


Figure 1: Distributions of the invariant mass, $m(pK^-\pi^+)$, in the range $2 < p_T < 10$ GeV/ c for (a) the forward data sample with $1.5 < y^* < 4.0$ and (b) the backward data sample with $-4.5 < y^* < -2.5$. The red dotted line is the inclusive Λ_c^+ candidates, the grey shaded area is the combinatorial background and the blue solid line is the sum of the two.

The fit is performed to the $\log_{10} \chi_{\text{IP}}^2(\Lambda_c^+)$ distribution of candidates within the mass interval $[M_{\Lambda_c^+} - 30 \text{ MeV}/c^2, M_{\Lambda_c^+} + 30 \text{ MeV}/c^2]$. The $\log_{10} \chi_{\text{IP}}^2(\Lambda_c^+)$ distribution of the combinatorial background is constructed from the sideband regions in data $[M_{\Lambda_c^+} - 50 \text{ MeV}/c^2, M_{\Lambda_c^+} - 30 \text{ MeV}/c^2]$ and $[M_{\Lambda_c^+} + 30 \text{ MeV}/c^2, M_{\Lambda_c^+} + 50 \text{ MeV}/c^2]$. Following LHCb charm cross-section measurements in pp collisions at $\sqrt{s} = 7$ TeV [22], the prompt Λ_c^+ and Λ_c^+ -from- b components are modelled independently with a Bukin function [36], which is defined as

$$f_{\text{Bukin}}(x; \mu, \sigma, \xi, \rho_L, \rho_R) \propto \begin{cases} \exp\left(-\ln 2 \left[\frac{\ln\left(1+2\xi\sqrt{\xi^2+1}\frac{x-\mu}{\sigma\sqrt{2\ln 2}}\right)}{\ln\left(1+2\xi^2-2\xi\sqrt{\xi^2+1}\right)}\right]^2\right) & x_L < x < x_R, \\ \exp\left(\frac{\xi\sqrt{\xi^2+1}(x-x_L)\sqrt{2\ln 2}}{\sigma(\sqrt{\xi^2+1}-\xi)^2 \ln(\sqrt{\xi^2+1}+\xi)} - \rho_L \left(\frac{x-x_L}{\mu-x_L}\right)^2 - \ln 2\right) & x < x_L, \\ \exp\left(-\frac{\xi\sqrt{\xi^2+1}(x-x_R)\sqrt{2\ln 2}}{\sigma(\sqrt{\xi^2+1}+\xi)^2 \ln(\sqrt{\xi^2+1}+\xi)} - \rho_R \left(\frac{x-x_R}{\mu-x_R}\right)^2 - \ln 2\right) & x > x_R, \end{cases} \quad (4)$$

where

$$x_{L,R} = \mu + \sigma\sqrt{2\ln 2} \left(\frac{\xi}{\sqrt{\xi^2+1}} \mp 1 \right). \quad (5)$$

The parameters μ and σ are the position and width of the peak, ρ_L and ρ_R are left and right tail exponential coefficients and ξ parameterises the asymmetry of the peak. The $\log_{10} \chi_{\text{IP}}^2(\Lambda_c^+)$ distribution in the simulation is compared to that in the data, where the signal $\log_{10} \chi_{\text{IP}}^2(\Lambda_c^+)$ distribution is obtained using the *sPlot* technique [37]. The simulated sample gives a good description of the shape of the prompt $\log_{10} \chi_{\text{IP}}^2(\Lambda_c^+)$ distribution, while slightly underestimating the prompt peak position μ . For the Λ_c^+ -from- b component, both μ and σ depend on p_T and y^* . The μ value in the data varies between 1.3 and 2.0, which is 0.3–0.5 larger than that in the simulation. The parameter μ in the prompt Bukin function and the parameters μ and σ in the Λ_c^+ -from- b Bukin function are determined from a fit to the data. The sum of the prompt and Λ_c^+ -from- b distributions of $\log_{10} \chi_{\text{IP}}^2(\Lambda_c^+)$ is obtained

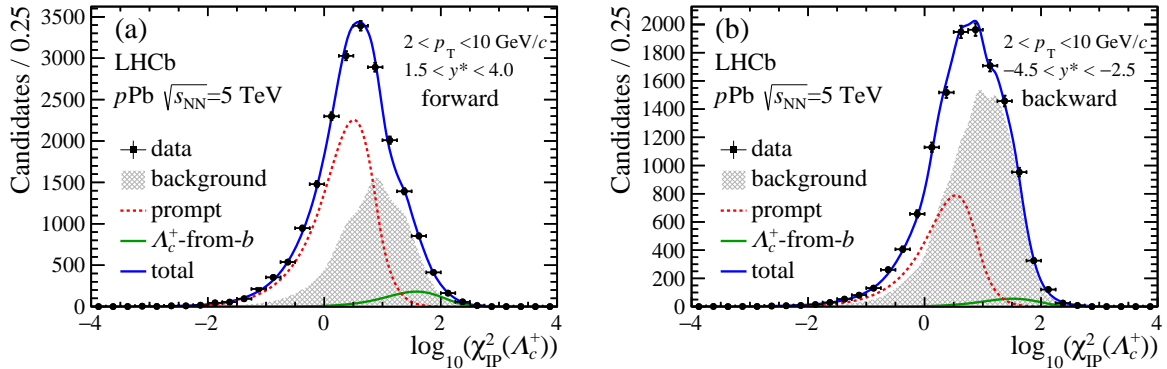


Figure 2: Distributions of $\log_{10} \chi_{\text{IP}}^2(\Lambda_c^+)$ in the range $2 < p_T < 10$ GeV/c with the fit results overlaid for (a) the forward data sample with $1.5 < y^* < 4.0$, and (b) the backward data sample with $-4.5 < y^* < -2.5$. The solid blue curve is the sum. The red dotted line is the prompt component, the green is the Λ_c^+ -from- b component and the grey shaded area denotes the combinatorial background.

with the *sPlot* technique using the invariant mass $m(pK^-\pi^+)$ as the discriminating variable, and is fitted with two Bukin functions. The correlation between the invariant mass $m(pK^-\pi^+)$ and $\log_{10} \chi_{\text{IP}}^2(\Lambda_c^+)$ is found to be negligible. For the prompt Bukin function, the parameter μ is a floating variable, while σ , ρ_L , ρ_R and ξ are fixed to the values determined from a fit to the simulation sample. For the Λ_c^+ -from- b Bukin function, the parameters μ and σ vary freely, while ρ_L , ρ_R and ξ are estimated from the simulation and can vary within their uncertainties.

Finally, the $\log_{10} \chi_{\text{IP}}^2(\Lambda_c^+)$ distribution is fitted with three components, two Bukin functions for the prompt Λ_c^+ and Λ_c^+ -from- b components respectively, where the parameters are determined as described above, and a background component derived from the sideband regions. The prompt fraction is determined independently in two-dimensional (p_T, y^*) bins and tends to decrease with increasing p_T and y^* , with an average value of $\sim 90\%$ for both rapidity regions. The $\log_{10} \chi_{\text{IP}}^2(\Lambda_c^+)$ distributions of Λ_c^+ candidates with $2 < p_T < 10$ GeV/c and in the full rapidity region, together with the fits, are displayed in Fig. 2 (a) and (b), for the forward and backward samples, respectively. The statistical uncertainty of the prompt fraction is considered to be partially correlated with the statistical uncertainty of the inclusive Λ_c^+ yield. The correlation factor in each (p_T, y^*) bin is derived from a simultaneous two-dimensional fit to the $m(pK^-\pi^+)$ - $\log_{10} \chi_{\text{IP}}^2(\Lambda_c^+)$ distribution.

The total efficiency, ε_{tot} , in Eq. 1 is decomposed into three components: the geometrical acceptance, the reconstruction and selection efficiency, and the PID efficiency. The geometrical acceptance efficiency is the fraction of Λ_c^+ baryons within the LHCb geometrical acceptance, and is determined from simulation. For most bins this efficiency is above 90%. The reconstruction and selection efficiencies are calculated with simulated $p\text{Pb}$ events at $\sqrt{s_{\text{NN}}} = 5$ TeV. The simulated samples are validated by comparing the distributions of kinematic variables with those obtained from the data using the *sPlot* technique. The reconstruction efficiency is affected by the track multiplicity of the event, which is not well reproduced in the simulation. Following the method developed in Ref. [10], the efficiency is evaluated as a function of track multiplicity and a correction factor is derived. The simulated samples do not model well Λ_c^+ decays through intermediate resonances $\Lambda(1520)$

and $K^*(892)^0$, which can result in local distortions of the $m(pK^-)$ and $m(K^-\pi^+)$ invariant-mass distributions. A method that uses $m(pK^-) - m(K^-\pi^+)$ as a two-dimensional weight to calculate the efficiencies is implemented [38] to take into account the effect of resonant structures in the Λ_c^+ decay, where the signal kinematics in the data are gained with the *sPlot* technique. The final reconstruction and selection efficiency in general increases with p_T . The efficiency is below 1% for the lowest p_T values and reaches 4–5% at $p_T > 8$ GeV/ c .

The PID efficiencies of the Λ_c^+ decay products are assessed separately with a data-driven method [24] using high-purity samples of D^0 mesons from $D^*(2010)^+$ decays for kaons and pions, and Λ baryons for protons. The samples are taken from the same p Pb data set as used in the present analysis. The single-track PID efficiencies are mostly above 80% (90%) for protons (pions and kaons) for track momenta in the range of $3 < p < 100$ GeV/ c and pseudorapidities in the range of $2 < \eta < 5$, although the efficiencies at the edge of the acceptance are generally lower. The single-track PID efficiencies are convolved with $\Lambda_c^+ \rightarrow pK^-\pi^+$ decay kinematic distributions obtained from simulation to produce the total PID efficiency for Λ_c^+ baryons in each (p_T, y^*) bin. The PID efficiency for Λ_c^+ baryons are 45–89% (46–74%) for the forward (backward) sample. The total efficiency is estimated to be 0.04–4.53% (0.07–2.87%) for the forward (backward) configuration.

3.3 Systematic uncertainties

The systematic uncertainties are evaluated separately for the forward and backward samples, unless otherwise specified. Sources of systematic uncertainty arising from the inclusive Λ_c^+ invariant-mass fit, the determination of the prompt Λ_c^+ fraction from the $\log_{10} \chi_{\text{IP}}^2(\Lambda_c^+)$ fit and the efficiency evaluations are studied independently for each (p_T, y^*) bin.

The systematic uncertainty of the inclusive Λ_c^+ invariant-mass fit is studied by replacing the fitting functions with a double Gaussian function with a common mean for the Λ_c^+ signal and an exponential function for the background. The relative uncertainty on the inclusive Λ_c^+ signals are 0.2–13.2% for the forward sample and 0.1–16.1% for the backward sample. The larger uncertainties are found in a few bins at the edge of acceptance where the yields are low. The uncertainty on the prompt fraction is evaluated by varying the width of the mass range used for the $\log_{10} \chi_{\text{IP}}^2(\Lambda_c^+)$ distribution to a wider ($[M_{\Lambda_c^+} - 35 \text{ MeV}/c^2, M_{\Lambda_c^+} + 35 \text{ MeV}/c^2]$) and a narrower ($[M_{\Lambda_c^+} - 20 \text{ MeV}/c^2, M_{\Lambda_c^+} + 20 \text{ MeV}/c^2]$) mass range. The uncertainty is estimated as the difference in the prompt fraction derived from the normal mass range and the alternative mass ranges. The uncertainties on the prompt fractions are 0.6–4.2% (0.7–19.0%) for the forward (backward) sample. The bins with the lowest p_T and largest $|y^*|$ have large uncertainties due to the high level of combinatorial background.

The relative uncertainty for the measured luminosity is 2.3% and 2.5% for the forward and backward samples [39], respectively. The branching fraction $\mathcal{B}(\Lambda_c^+ \rightarrow pK^-\pi^+) = (6.35 \pm 0.33)\%$ [34] yields a relative uncertainty of 5.2%.

The uncertainty on the efficiency correction originates from several sources: (1) the uncertainty in correcting the track multiplicity distributions in the simulation (5.6% in the forward region and 5.8% in the backward region); (2) the uncertainty arising from the simulation description of $\Lambda_c^+ \rightarrow pK^-\pi^+$ decay resonant structures (forward: 3.0%, backward: 4.0%); (3) the uncertainty in the PID efficiency (forward: 0.5–4.3%, backward: 0.5–10.4%); and (4) the limited size of the simulated sample (forward: 4.2–27.0%, backward:

4.3–26.0%).

All the systematic uncertainties considered for the differential cross-sections are listed in Table 1. For the total cross-section, the uncertainties due to the simulated sample size are considered to be fully uncorrelated for each (p_T, y^*) bin and are summed in quadrature. The uncertainties on the luminosity and the $\Lambda_c^+ \rightarrow pK^-\pi^+$ branching fraction are fully correlated among (p_T, y^*) bins. The other systematic uncertainties are found to be almost fully correlated across the bins and are summed linearly.

For the R_{FB} ratio, the common uncertainty on $\mathcal{B}(\Lambda_c^+ \rightarrow pK^-\pi^+)$ cancels out. The systematic uncertainty on the raw Λ_c^+ yields is considered uncorrelated because of different levels of background in the forward and backward data samples. The systematic uncertainties on the reconstruction and selection efficiency are assumed to be fully correlated except for the uncertainty due to the Λ_c^+ decay resonant structures, which is uncorrelated. The uncertainty on the PID efficiency is assumed to be 90% correlated. The luminosity uncertainties are considered uncorrelated. For the $R_{\Lambda_c^+/D^0}$ ratio, all systematic uncertainties are uncorrelated except for the luminosity uncertainty which cancels out.

Table 1: Systematic and statistical uncertainties for the differential cross-sections. The ranges indicate the variation over the (p_T, y^*) bins.

Source	Relative uncertainty (%)	
	Forward	Backward
Correlated between bins		
Invariant mass fit	0.2–13.2	0.1–16.1
Prompt fraction	0.6–4.2	0.7–19.0
Luminosity	2.3	2.5
$\mathcal{B}(\Lambda_c^+ \rightarrow pK^-\pi^+)$	5.2	5.2
Multiplicity correction	5.6	5.8
Λ_c^+ decay resonant structures	3.0	4.0
PID efficiency	0.5–4.3	0.5–10.4
Uncorrelated between bins		
Simulation sample size	4.2–27.0	4.3–26.0
Statistical uncertainty	3.6–42.5	6.2–44.3

4 Results

4.1 Prompt Λ_c^+ cross-section

The double-differential cross-section of prompt Λ_c^+ production in $p\text{Pb}$ collisions at 5.02 TeV is measured as a function of the p_T and y^* of the Λ_c^+ baryon. The results are displayed in Fig. 3, and the corresponding numerical values are shown in Table 4 of Appendix A.

The double-differential cross-section is integrated over p_T between 2 and 10 GeV/ c to obtain the differential cross-section as a function of y^* . Likewise, integrating over y^* in regions $2.5 < |y^*| < 4.0$ (the common $|y^*|$ region of the forward and backward data), $1.5 < y^* < 4.0$ (for the forward data) and $-4.5 < y^* < -2.5$ (for the backward data) yields the differential cross-section as a function of p_T . The differential cross-sections $d\sigma/dy^*$ versus y^* and $d\sigma/dp_T$ versus p_T are shown in Fig. 4. The corresponding values are shown in Appendix A.

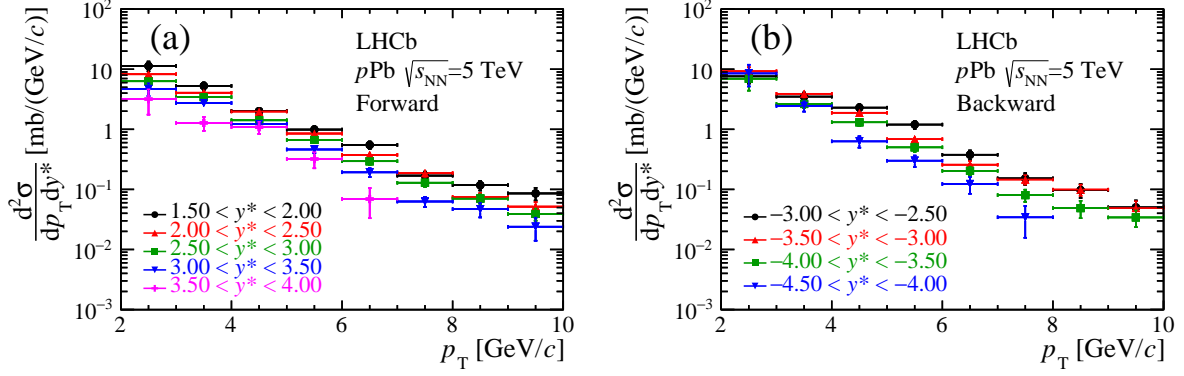


Figure 3: Double-differential cross-section of prompt Λ_c^+ baryons in $p\text{Pb}$ collisions in the (a) forward and (b) backward collision samples. The uncertainty represents the quadratic sum of the statistical and the systematic uncertainties.

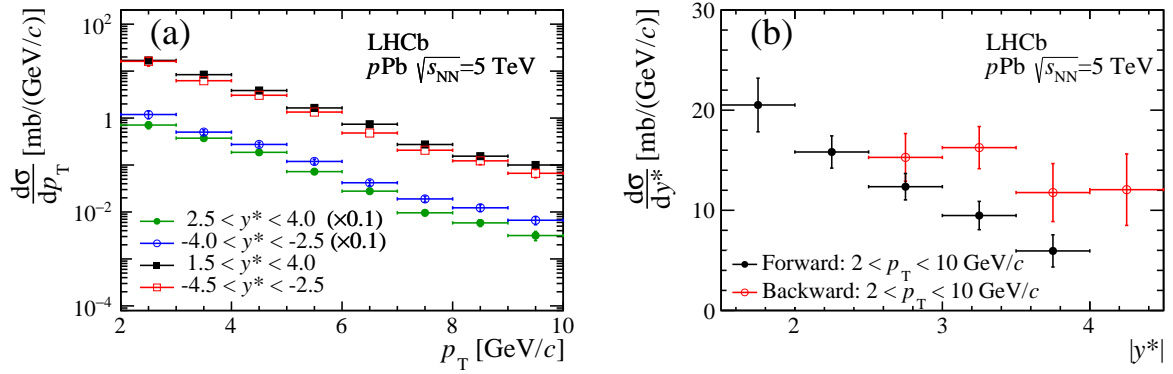


Figure 4: Differential cross-section of prompt Λ_c^+ baryons in $p\text{Pb}$ collisions as a function of (a) p_T and (b) y^* in the forward and backward samples. The forward and backward differential cross-sections $d\sigma/dp_T$ in the common rapidity region $2.5 < |y^*| < 4.0$ are scaled by 0.1 to improve the visibility. The box on each point represents the systematic uncertainty and the error bar represents the sum in quadrature of the statistical and the systematic uncertainties.

For the full kinematic range, the total cross-section is determined to be

$$\begin{aligned} \sigma(2 < p_T < 10 \text{ GeV}/c, 1.5 < y^* < 4.0) &= 32.1 \pm 1.1 \pm 3.2 \text{ mb}, \\ \sigma(2 < p_T < 10 \text{ GeV}/c, -4.5 < y^* < -2.5) &= 27.7 \pm 1.8 \pm 3.9 \text{ mb}. \end{aligned}$$

where the first uncertainties are statistical and the second systematic. The correlated components in the systematic uncertainties are 2.7 mb and 2.6 mb for the forward and backward data, respectively.

4.2 R_{FB} ratio

The total cross-section in the common rapidity region between the forward and backward samples is also obtained to calculate the prompt Λ_c^+ R_{FB} ratio,

$$\begin{aligned} \sigma(2 < p_T < 10 \text{ GeV}/c, 2.5 < y^* < 4.0) &= 13.9 \pm 0.8 \pm 1.5 \text{ mb}, \\ \sigma(2 < p_T < 10 \text{ GeV}/c, -4.0 < y^* < -2.5) &= 21.7 \pm 1.2 \pm 2.8 \text{ mb}. \end{aligned}$$

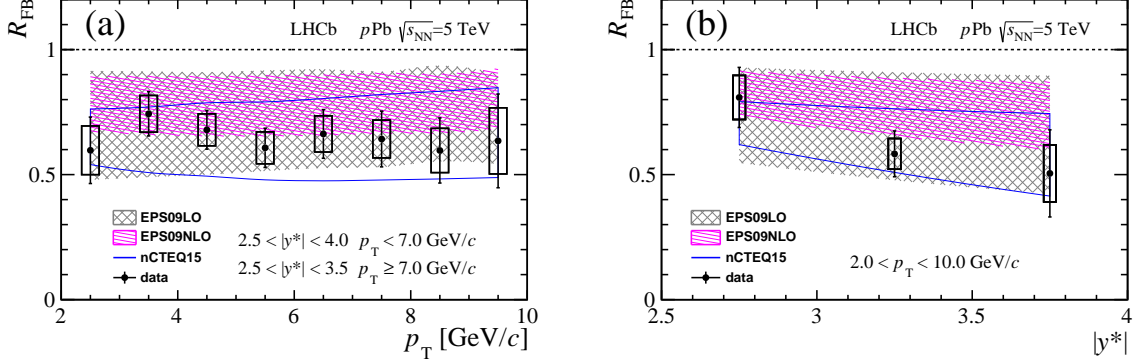


Figure 5: (a) Forward-backward production ratios R_{FB} as a function of p_T integrated over $2.5 < |y^*| < 4.0$ for p_T less than 7 GeV/c and $2.5 < |y^*| < 3.5$ for p_T greater than 7 GeV/c, and (b) R_{FB} as a function of y^* integrated over $2 < p_T < 10$ GeV/c. The box on each point represents the systematic uncertainty and the error bar represents the sum in quadrature of the statistical and the systematic uncertainties.

Figure 5(a) shows the prompt Λ_c^+ R_{FB} ratio as a function of p_T in the region common to both forward and backward samples, $2.5 < |y^*| < 4.0$. In the rapidity region $3.5 < y^* < 4.0$, the forward data have no measurement for $p_T > 7.0$ GeV/c. For p_T beyond 7 GeV/c, the R_{FB} ratio is therefore calculated with both forward and backward cross-sections in the region $2.5 < |y^*| < 3.5$. Figure 5(b) shows the R_{FB} ratio as a function of $|y^*|$ in the region $2 < p_T < 10$ GeV/c. The measurement is in agreement with calculations using the HELAC-Onia generator [40–42], which incorporates the parton distribution functions of EPS09LO, EPS09NLO [43] and nCTEQ15 [44]. The numerical values are given in Appendix B.

4.3 Λ_c^+ to D^0 cross-section ratio, $R_{\Lambda_c^+/D^0}$

The ratio of the production cross-sections between prompt Λ_c^+ baryons and D^0 mesons is calculated as a function of the p_T and y^* of the hadrons using the previous measurement of D^0 production cross-section [10]. The results are compared to the HELAC-Onia calculations [40–42], which are based on a data-driven modelling of parton scattering. The theory prediction is calculated with HELAC-Onia, where the Λ_c^+ production cross-section is parameterised by fitting the LHCb pp data [22]. The nuclear matter effects in pPb collisions are incorporated using the nPDFs EPS09LO/NLO [43], nCTEQ15 nPDFs [44]. The effects of the nPDFs tend to cancel in the ratio $R_{\Lambda_c^+/D^0}$, leading to similar ratios between the different nPDFs. The calculations with the three nPDFs show comparable trends and values across p_T and y^* , with nCTEQ15 slightly lower than EPS09, suggesting small nPDF effects in the $R_{\Lambda_c^+/D^0}$ ratio.

Figure 6 shows the $R_{\Lambda_c^+/D^0}$ ratio as a function of p_T in four different rapidity ranges. Numerical values can be found in Table 7 in Appendix C. The $R_{\Lambda_c^+/D^0}$ ratios are measured to be around 0.3. The values are larger at lower p_T (< 5 GeV/c) and tend to decrease for p_T greater than 5 GeV/c. The trend is less clear in the backward region due to larger uncertainties. The theoretical calculations are displayed as coloured curves. They increase slightly with increasing p_T . In the backward region, the data points are consistent with the

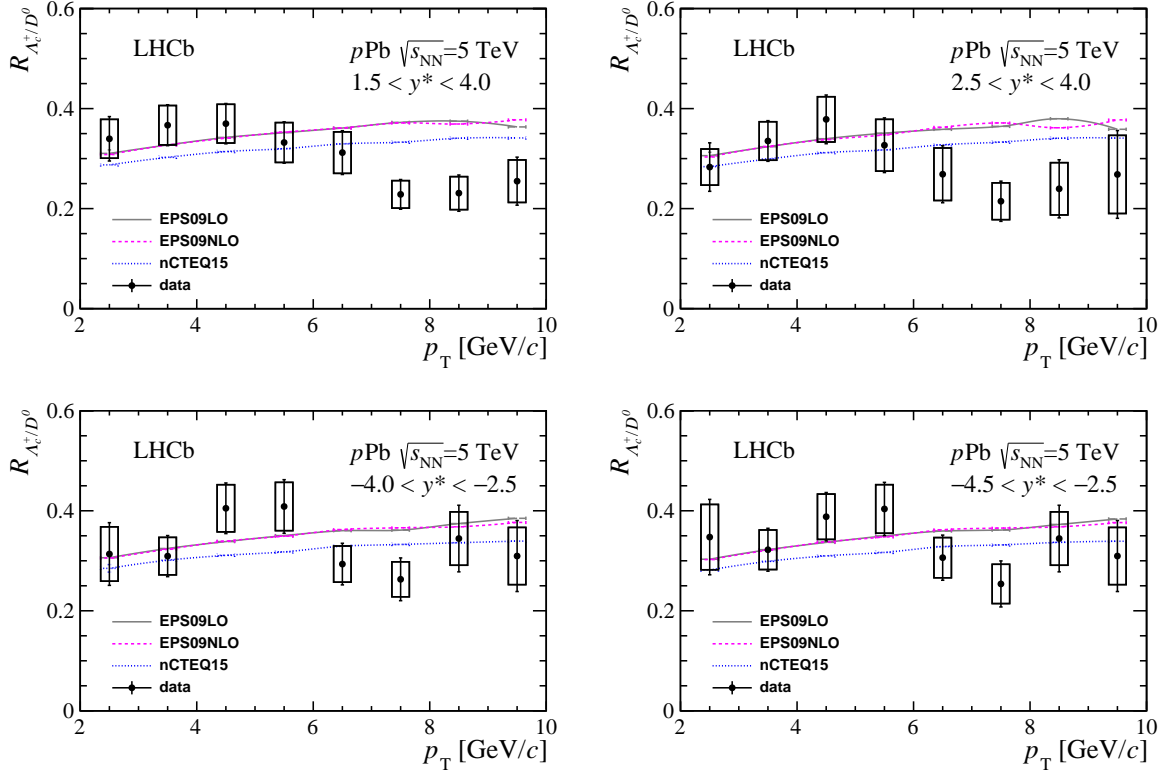


Figure 6: The cross-section ratio $R_{\Lambda_c^+/D^0}$ between Λ_c^+ baryons and D^0 mesons as a function of p_T integrated over four different rapidity regions. The box on each point represents the systematic uncertainty and the error bar represents the sum in quadrature of the statistical and the systematic uncertainties. The coloured curves represent HELAC-Onia calculations with nPDF EPS09LO/NLO and nCTEQ15.

theoretical calculations. The forward data points are consistent with the calculations at lower p_T (< 7 GeV/c). However, they are below the theoretical predictions for p_T greater than 7 GeV/c.

Figure 7 illustrates the $R_{\Lambda_c^+/D^0}$ ratio for $2 < p_T < 10$ GeV/c as a function of rapidity. The numerical values are given in Appendix C. The theoretical calculations are made for the rapidity range $-4.0 < y^* < 4.0$, and show a relatively uniform distribution. Both the forward and backward data are consistent with the theoretical predictions for the full rapidity range.

The ALICE collaboration has recently reported a measurement of the prompt Λ_c^+ baryons in pPb collisions at $\sqrt{s_{NN}} = 5.02$ TeV [21]. Their $R_{\Lambda_c^+/D^0}$ ratio in the midrapidity region for $2 < p_T < 12$ GeV/c and $-0.96 < y^* < 0.04$ is measured to be $0.602 \pm 0.060_{-0.087}^{+0.159}$, and is shown in Fig. 7. The value is larger than the ratios shown in the solid points in both forward and backward rapidity regions. In the forward region, the $R_{\Lambda_c^+/D^0}$ ratio tends to increase with decreasing y^* , suggesting a trend that can be compatible with the ALICE measurement. In the backward region, however, no clear trend is observed due to large uncertainties.

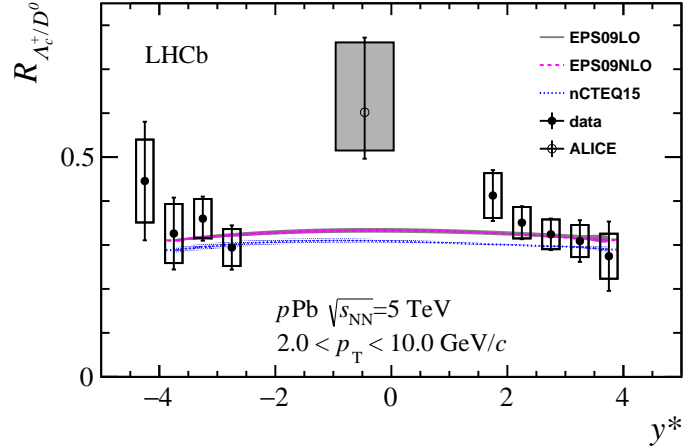


Figure 7: The cross-section ratio $R_{\Lambda_c^+/D^0}$ between Λ_c^+ baryons and D^0 mesons as a function of y^* integrated over $2 < p_T < 10$ GeV/c. The box on each point represents the systematic uncertainty and the error bar represents the sum in quadrature of the statistical and the systematic uncertainties. The coloured curves show HELAC-Onia calculations incorporating nPDFs EPS09LO/NLO and nCTEQ15. The open circle is the value measured by the ALICE collaboration [21]. The error bar shows the total uncertainty and the grey square the systematic.

5 Conclusion

Prompt Λ_c^+ production cross-sections are measured with p Pb collision data collected by the LHCb detector at $\sqrt{s_{NN}} = 5.02$ TeV. The forward-backward production ratios R_{FB} are presented, and are compared to theoretical predictions. A larger production rate in the backward-rapidity region compared to the forward region is observed. The forward-backward production ratio R_{FB} shows consistency with HELAC-Onia calculations with the three nPDFs EPS09LO, EPS09NLO [43] and nCTEQ15 [44]. In addition, the production cross-section ratio $R_{\Lambda_c^+/D^0}$ between Λ_c^+ baryons and D^0 mesons, which is sensitive to the hadronisation mechanism of the charm particles, is measured. The result is consistent with theory calculations based on pp data. The Λ_c^+ measurements in classes of event multiplicity can be anticipated with the p Pb dataset at $\sqrt{s_{NN}} = 8.16$ TeV recorded by the LHCb collaboration in 2016, which is about 20 times larger than the 5.02 TeV dataset. An improvement in precision is also achievable with the increased sample size and an improved simulation. In addition, a dataset of pp collisions at $\sqrt{s} = 5.02$ TeV corresponding to a luminosity of 0.1 fb^{-1} was collected in 2017. The nuclear modification factor for the Λ_c^+ baryons can be directly measured using this dataset.

Acknowledgements

We are grateful to H. Shao for providing theoretical calculations of prompt Λ_c^+ production in p Pb collisions in the LHCb acceptance. We express our gratitude to our colleagues in the CERN accelerator departments for the excellent performance of the LHC. We thank the technical and administrative staff at the LHCb institutes. We acknowledge support from CERN and from the national agencies: CAPES, CNPq, FAPERJ and FINEP (Brazil);

MOST and NSFC (China); CNRS/IN2P3 (France); BMBF, DFG and MPG (Germany); INFN (Italy); NWO (Netherlands); MNiSW and NCN (Poland); MEN/IFA (Romania); MSHE (Russia); MinECo (Spain); SNSF and SER (Switzerland); NASU (Ukraine); STFC (United Kingdom); NSF (USA). We acknowledge the computing resources that are provided by CERN, IN2P3 (France), KIT and DESY (Germany), INFN (Italy), SURF (Netherlands), PIC (Spain), GridPP (United Kingdom), RRCKI and Yandex LLC (Russia), CSCS (Switzerland), IFIN-HH (Romania), CBPF (Brazil), PL-GRID (Poland) and OSC (USA). We are indebted to the communities behind the multiple open-source software packages on which we depend. Individual groups or members have received support from AvH Foundation (Germany); EPLANET, Marie Skłodowska-Curie Actions and ERC (European Union); ANR, Labex P2IO and OCEVU, and Région Auvergne-Rhône-Alpes (France); Key Research Program of Frontier Sciences of CAS, CAS PIFI, and the Thousand Talents Program (China); RFBR, RSF and Yandex LLC (Russia); GVA, XuntaGal and GENCAT (Spain); the Royal Society and the Leverhulme Trust (United Kingdom); Laboratory Directed Research and Development program of LANL (USA).

Appendices

A Numerical values of the Λ_c^+ cross-sections

Table 2: Measured differential cross-section (in $\text{mb}/(\text{GeV}/c)$) of prompt Λ_c^+ baryons as a function of p_T in $p\text{Pb}$ forward and backward data in different rapidity regions. The right column shows the results for $p_T > 7 \text{ GeV}/c$ and $2.5 < |y^*| < 3.5$, which are used to compute the R_{FB} values at $p_T > 7 \text{ GeV}/c$. The first uncertainties are statistical and the second are systematic.

Forward ($\text{mb}/(\text{GeV}/c)$)			
p_T [GeV/c]	$y^* \in [1.5, 4.0]$	$y^* \in [2.5, 4.0]$	$y^* \in [2.5, 3.5]$
[2, 3]	$16.886 \pm 1.066 \pm 1.811$	$7.107 \pm 0.812 \pm 0.875$	—
[3, 4]	$8.402 \pm 0.250 \pm 0.844$	$3.731 \pm 0.142 \pm 0.401$	—
[4, 5]	$3.859 \pm 0.113 \pm 0.368$	$1.864 \pm 0.087 \pm 0.194$	—
[5, 6]	$1.644 \pm 0.052 \pm 0.165$	$0.724 \pm 0.036 \pm 0.080$	—
[6, 7]	$0.740 \pm 0.030 \pm 0.074$	$0.278 \pm 0.020 \pm 0.031$	—
[7, 8]	$0.274 \pm 0.013 \pm 0.027$	—	$0.096 \pm 0.007 \pm 0.011$
[8, 9]	$0.154 \pm 0.010 \pm 0.017$	—	$0.059 \pm 0.006 \pm 0.008$
[9, 10]	$0.100 \pm 0.008 \pm 0.013$	—	$0.032 \pm 0.004 \pm 0.006$
Backward ($\text{mb}/(\text{GeV}/c)$)			
p_T [GeV/c]	$y^* \in [-4.5, -2.5]$	$y^* \in [-4.0, -2.5]$	$y^* \in [-3.5, -2.5]$
[2, 3]	$16.162 \pm 1.750 \pm 2.890$	$11.902 \pm 1.180 \pm 1.940$	—
[3, 4]	$6.248 \pm 0.318 \pm 0.688$	$5.021 \pm 0.271 \pm 0.546$	—
[4, 5]	$3.059 \pm 0.132 \pm 0.321$	$2.744 \pm 0.122 \pm 0.288$	—
[5, 6]	$1.342 \pm 0.070 \pm 0.143$	$1.192 \pm 0.067 \pm 0.127$	—
[6, 7]	$0.481 \pm 0.031 \pm 0.054$	$0.419 \pm 0.029 \pm 0.046$	—
[7, 8]	$0.207 \pm 0.019 \pm 0.024$	$0.190 \pm 0.017 \pm 0.021$	$0.048 \pm 0.032 \pm 0.419$
[8, 9]	—	$0.123 \pm 0.014 \pm 0.016$	$0.019 \pm 0.031 \pm 0.010$
[9, 10]	—	$0.067 \pm 0.009 \pm 0.010$	$0.046 \pm 7.500 \pm 0.000$

Table 3: Differential cross-section (in mb) for prompt Λ_c^+ baryons as a function of $|y^*|$ in $p\text{Pb}$ forward and backward data. The first uncertainties are statistical and the second are systematic.

Forward (mb)	
$ y^* $	$p_T \in [2, 10]$ [GeV/c]
[1.5, 2.0]	$20.517 \pm 1.359 \pm 2.311$
[2.0, 2.5]	$15.823 \pm 0.511 \pm 1.528$
[2.5, 3.0]	$12.358 \pm 0.451 \pm 1.240$
[3.0, 3.5]	$9.479 \pm 0.928 \pm 1.065$
[3.5, 4.0]	$5.943 \pm 1.299 \pm 0.949$
Backward (mb)	
$ y^* $	$p_T \in [2, 10]$ [GeV/c]
[2.5, 3.0]	$15.283 \pm 1.438 \pm 1.900$
[3.0, 3.5]	$16.260 \pm 1.024 \pm 1.838$
[3.5, 4.0]	$11.772 \pm 1.684 \pm 2.356$
[4.0, 4.5]	$12.060 \pm 2.608 \pm 2.438$

Table 4: Double-differential cross-section (in $\text{mb}/(\text{GeV}/c)$) for prompt Λ_c^+ baryons as a function of p_T and y^* in $p\text{Pb}$ forward and backward data. The first uncertainty is statistical and the second is systematic.

p_T [GeV/c]	Forward (mb/(GeV/c))				
	$y^* \in [1.5, 2.0]$	$y^* \in [2.0, 2.5]$	$y^* \in [2.5, 3.0]$	$y^* \in [3.0, 3.5]$	$y^* \in [3.5, 4.0]$
[2, 3]	$11.316 \pm 1.296 \pm 1.634$	$8.241 \pm 0.481 \pm 0.893$	$6.304 \pm 0.426 \pm 0.716$	$4.721 \pm 0.914 \pm 0.680$	$3.189 \pm 1.272 \pm 0.667$
[3, 4]	$5.280 \pm 0.382 \pm 0.626$	$4.062 \pm 0.150 \pm 0.407$	$3.444 \pm 0.132 \pm 0.363$	$2.742 \pm 0.142 \pm 0.297$	$1.277 \pm 0.208 \pm 0.258$
[4, 5]	$2.009 \pm 0.126 \pm 0.223$	$1.982 \pm 0.072 \pm 0.194$	$1.412 \pm 0.054 \pm 0.137$	$1.228 \pm 0.066 \pm 0.133$	$1.087 \pm 0.150 \pm 0.194$
[5, 6]	$0.990 \pm 0.066 \pm 0.120$	$0.851 \pm 0.037 \pm 0.086$	$0.665 \pm 0.033 \pm 0.069$	$0.462 \pm 0.030 \pm 0.055$	$0.321 \pm 0.057 \pm 0.077$
[6, 7]	$0.549 \pm 0.040 \pm 0.067$	$0.375 \pm 0.020 \pm 0.040$	$0.294 \pm 0.018 \pm 0.032$	$0.192 \pm 0.019 \pm 0.026$	$0.069 \pm 0.029 \pm 0.021$
[7, 8]	$0.170 \pm 0.018 \pm 0.021$	$0.186 \pm 0.012 \pm 0.021$	$0.129 \pm 0.011 \pm 0.016$	$0.063 \pm 0.009 \pm 0.009$	–
[8, 9]	$0.117 \pm 0.013 \pm 0.017$	$0.074 \pm 0.007 \pm 0.010$	$0.070 \pm 0.007 \pm 0.010$	$0.047 \pm 0.009 \pm 0.009$	–
[9, 10]	$0.086 \pm 0.013 \pm 0.016$	$0.052 \pm 0.006 \pm 0.008$	$0.039 \pm 0.006 \pm 0.007$	$0.024 \pm 0.006 \pm 0.008$	–
p_T [GeV/c]	Backward (mb/(GeV/c))				
	$y^* \in [-4.5, -4.0]$	$y^* \in [-4.0, -3.5]$	$y^* \in [-3.5, -3.0]$	$y^* \in [-3.0, -2.5]$	
[2, 3]	$8.519 \pm 2.585 \pm 2.138$	$6.957 \pm 1.666 \pm 1.938$	$9.236 \pm 0.977 \pm 1.177$	$7.610 \pm 1.358 \pm 1.242$	
[3, 4]	$2.453 \pm 0.331 \pm 0.351$	$2.638 \pm 0.223 \pm 0.318$	$3.902 \pm 0.276 \pm 0.439$	$3.502 \pm 0.410 \pm 0.421$	
[4, 5]	$0.630 \pm 0.101 \pm 0.090$	$1.309 \pm 0.091 \pm 0.158$	$1.885 \pm 0.118 \pm 0.203$	$2.295 \pm 0.194 \pm 0.267$	
[5, 6]	$0.300 \pm 0.045 \pm 0.047$	$0.501 \pm 0.048 \pm 0.063$	$0.684 \pm 0.054 \pm 0.076$	$1.199 \pm 0.112 \pm 0.145$	
[6, 7]	$0.123 \pm 0.025 \pm 0.029$	$0.203 \pm 0.023 \pm 0.026$	$0.258 \pm 0.026 \pm 0.030$	$0.377 \pm 0.045 \pm 0.049$	
[7, 8]	$0.034 \pm 0.015 \pm 0.011$	$0.080 \pm 0.014 \pm 0.013$	$0.146 \pm 0.018 \pm 0.019$	$0.152 \pm 0.026 \pm 0.021$	
[8, 9]	–	$0.049 \pm 0.011 \pm 0.011$	$0.099 \pm 0.015 \pm 0.015$	$0.097 \pm 0.020 \pm 0.016$	
[9, 10]	–	$0.034 \pm 0.006 \pm 0.009$	$0.049 \pm 0.011 \pm 0.010$	$0.050 \pm 0.012 \pm 0.009$	

B Numerical values of Λ_c^+ R_{FB} ratios

Table 5: Forward-backward prompt Λ_c^+ production ratio R_{FB} as a function of p_{T} in the common range $2.5 < |y^*| < 4.0$. The first uncertainty is statistical and the second is systematic.

$p_{\text{T}}[\text{GeV}/c]$	R_{FB}
[2, 3]	$0.60 \pm 0.09 \pm 0.10$
[3, 4]	$0.74 \pm 0.05 \pm 0.07$
[4, 5]	$0.68 \pm 0.04 \pm 0.06$
[5, 6]	$0.61 \pm 0.05 \pm 0.06$
[6, 7]	$0.66 \pm 0.07 \pm 0.07$
[7, 8]	$0.64 \pm 0.08 \pm 0.08$
[8, 9]	$0.60 \pm 0.10 \pm 0.09$
[9, 10]	$0.63 \pm 0.13 \pm 0.13$

Table 6: R_{FB} ratio as a function of $|y^*|$ in the range $2 < p_{\text{T}} < 10 \text{ GeV}/c$. The first uncertainty is statistical and the second is systematic.

y^*	R_{FB}
[2.5, 3.0]	$0.81 \pm 0.08 \pm 0.09$
[3.0, 3.5]	$0.58 \pm 0.07 \pm 0.06$
[3.5, 4.0]	$0.50 \pm 0.13 \pm 0.11$

C Numerical values of $R_{\Lambda_c^+/D^0}$ ratios

Table 7: Production ratio $R_{\Lambda_c^+/D^0}$ as a function of p_T in the forward and backward rapidity regions. The first uncertainty is statistical and the second is systematic.

Forward		
p_T [GeV/c]	$y^* \in [2.5, 4.0]$	$y^* \in [1.5, 4.0]$
[2, 3]	$0.283 \pm 0.032 \pm 0.036$	$0.340 \pm 0.021 \pm 0.039$
[3, 4]	$0.335 \pm 0.013 \pm 0.039$	$0.367 \pm 0.011 \pm 0.039$
[4, 5]	$0.378 \pm 0.018 \pm 0.045$	$0.370 \pm 0.011 \pm 0.039$
[5, 6]	$0.327 \pm 0.017 \pm 0.052$	$0.332 \pm 0.011 \pm 0.040$
[6, 7]	$0.269 \pm 0.022 \pm 0.053$	$0.312 \pm 0.014 \pm 0.042$
[7, 8]	$0.215 \pm 0.016 \pm 0.037$	$0.228 \pm 0.011 \pm 0.028$
[8, 9]	$0.240 \pm 0.025 \pm 0.052$	$0.231 \pm 0.015 \pm 0.033$
[9, 10]	$0.268 \pm 0.040 \pm 0.078$	$0.255 \pm 0.022 \pm 0.043$
Backward		
p_T [GeV/c]	$y^* \in [-4.0, -2.5]$	$y^* \in [-4.5, -2.5]$
[2, 3]	$0.314 \pm 0.031 \pm 0.054$	$0.347 \pm 0.038 \pm 0.065$
[3, 4]	$0.309 \pm 0.017 \pm 0.037$	$0.322 \pm 0.016 \pm 0.040$
[4, 5]	$0.405 \pm 0.018 \pm 0.047$	$0.388 \pm 0.017 \pm 0.045$
[5, 6]	$0.409 \pm 0.023 \pm 0.048$	$0.404 \pm 0.022 \pm 0.049$
[6, 7]	$0.293 \pm 0.021 \pm 0.036$	$0.306 \pm 0.020 \pm 0.040$
[7, 8]	$0.263 \pm 0.025 \pm 0.035$	$0.254 \pm 0.024 \pm 0.039$
[8, 9]	$0.344 \pm 0.040 \pm 0.053$	$0.344 \pm 0.040 \pm 0.053$
[9, 10]	$0.310 \pm 0.042 \pm 0.057$	$0.310 \pm 0.042 \pm 0.057$

Table 8: Production ratio $R_{\Lambda_c^+/D^0}$ as a function of y^* for $2 < p_T < 10$ GeV/c. The first uncertainty is statistical and the second is systematic.

$ y^* $	$2.0 < p_T < 10.0$ [GeV/c]
[-4.5, -4.0]	$0.446 \pm 0.096 \pm 0.094$
[-4.0, -3.5]	$0.326 \pm 0.047 \pm 0.067$
[-3.5, -3.0]	$0.360 \pm 0.023 \pm 0.045$
[-3.0, -2.5]	$0.294 \pm 0.028 \pm 0.042$
[1.5, 2.0]	$0.413 \pm 0.027 \pm 0.051$
[2.0, 2.5]	$0.351 \pm 0.011 \pm 0.036$
[2.5, 3.0]	$0.324 \pm 0.012 \pm 0.034$
[3.0, 3.5]	$0.309 \pm 0.030 \pm 0.036$
[3.5, 4.0]	$0.274 \pm 0.060 \pm 0.051$

References

- [1] Y. Akiba *et al.*, *The hot QCD white paper: Exploring the phases of QCD at RHIC and the LHC*, [arXiv:1502.02730](#).
- [2] STAR collaboration, L. Adamczyk *et al.*, *Observation of D^0 meson nuclear modifications in Au+Au collisions at $\sqrt{s_{NN}} = 200$ GeV*, Phys. Rev. Lett. **113** (2014) 142301, [arXiv:1404.6185](#).
- [3] ALICE collaboration, B. B. Abelev *et al.*, *Azimuthal anisotropy of D -meson production in Pb-Pb collisions at $\sqrt{s_{NN}} = 2.76$ TeV*, Phys. Rev. **C90** (2014) 034904, [arXiv:1405.2001](#).
- [4] D. Kharzeev and K. Tuchin, *Signatures of the color glass condensate in J/ψ production off nuclear targets*, Nucl. Phys. **A770** (2006) 40, [arXiv:hep-ph/0510358](#).
- [5] H. Fujii, F. Gelis, and R. Venugopalan, *Quark pair production in high energy pA collisions: General features*, Nucl. Phys. **A780** (2006) 146, [arXiv:hep-ph/0603099](#).
- [6] S. Gavin and J. Milana, *Energy loss at large x_F in nuclear collisions*, Phys. Rev. Lett. **68** (1992) 1834.
- [7] R. Vogt, *x_F dependence of ψ and Drell-Yan production*, Phys. Rev. **C61** (2000) 035203, [arXiv:hep-ph/9907317](#).
- [8] F. Arleo and S. Peigné, *Heavy-quarkonium suppression in $p-A$ collisions from parton energy loss in cold QCD matter*, JHEP **03** (2013) 122, [arXiv:1212.0434](#).
- [9] F. Arleo and V.-N. Tram, *A systematic study of J/ψ suppression in cold nuclear matter*, Eur. Phys. J. **C55** (2008) 449, [arXiv:hep-ph/0612043](#).
- [10] LHCb collaboration, R. Aaij *et al.*, *Study of prompt D^0 meson production in pPb collisions at $\sqrt{s_{NN}} = 5$ TeV*, JHEP **10** (2017) 090, [arXiv:1707.02750](#).
- [11] Y. Oh, C. M. Ko, S. H. Lee, and S. Yasui, *Ratios of heavy baryons to heavy mesons in relativistic nucleus-nucleus collisions*, Phys. Rev. **C79** (2009) 044905, [arXiv:0901.1382](#).
- [12] S. H. Lee *et al.*, *Λ_c enhancement from strongly coupled quark-gluon plasma*, Phys. Rev. Lett. **100** (2008) 222301, [arXiv:0709.3637](#).
- [13] M. A. C. Lamont and the STAR Collaboration, *Recent results on strangeness production at rhic*, J. Phys. G **32** (2006) S105, [arXiv:nucl-ex/0608017](#).
- [14] ALICE collaboration, B. Abelev *et al.*, *K_s^0 and Λ production in Pb-Pb collisions at $\sqrt{s_{NN}} = 2.76$ TeV*, Phys. Rev. Lett. **111** (2013) 222301, [arXiv:1307.5530](#).
- [15] R. C. Hwa and C. B. Yang, *Strangeness enhancement in the parton model*, Phys. Rev. **C66** (2002) 064903, [arXiv:nucl-th/0206005](#).
- [16] V. Greco, C. M. Ko, and P. Lévai, *Parton coalescence and antiproton/pion anomaly at RHIC*, Phys. Rev. Lett. **90** (2003) 202302, [arXiv:nucl-th/0301093](#).

- [17] R. J. Fries, B. Müller, C. Nonaka, and S. A. Bass, *Hadronization in heavy-ion collisions: recombination and fragmentation of partons*, Phys. Rev. Lett. **90** (2003) 202303, arXiv:nuc1-th/0301087.
- [18] D. Molnár and S. A. Voloshin, *Elliptic flow at large transverse momenta from quark coalescence*, Phys. Rev. Lett. **91** (2003) 092301, arXiv:nuc1-th/0302014.
- [19] G. Xie, Λ_c production in Au+Au collisions at $\sqrt{s_{NN}} = 200$ GeV measured by the STAR experiment, Nuclear Physics A **967** (2017) 928, arXiv:1704.04353.
- [20] ALICE, S. Acharya *et al.*, Λ_c^+ production in Pb-Pb collisions at $\sqrt{s_{NN}} = 5.02$ TeV, arXiv:1809.10922.
- [21] ALICE collaboration, S. Acharya *et al.*, Λ_c^+ production in pp collisions at $\sqrt{s} = 7$ TeV and in p-Pb collisions at $\sqrt{s_{NN}} = 5.02$ TeV, JHEP **04** (2018) 108, arXiv:1712.09581.
- [22] LHCb collaboration, R. Aaij *et al.*, *Prompt charm production in pp collisions at $\sqrt{s} = 7$ TeV*, Nucl. Phys. **B871** (2013) 1, arXiv:1302.2864.
- [23] LHCb collaboration, A. A. Alves Jr. *et al.*, *The LHCb detector at the LHC*, JINST **3** (2008) S08005.
- [24] LHCb collaboration, R. Aaij *et al.*, *LHCb detector performance*, Int. J. Mod. Phys. **A30** (2015) 1530022, arXiv:1412.6352.
- [25] LHCb collaboration, R. Aaij *et al.*, *Study of J/ψ production and cold nuclear matter effects in pPb collisions at $\sqrt{s_{NN}} = 5$ TeV*, JHEP **02** (2014) 072, arXiv:1308.6729.
- [26] T. Sjöstrand, S. Mrenna, and P. Skands, *A brief introduction to PYTHIA 8.1*, Comput. Phys. Commun. **178** (2008) 852, arXiv:0710.3820.
- [27] S. Porteboeuf, T. Pierog, and K. Werner, *Producing hard processes regarding the complete event: the EPOS event generator*, in *Proceedings, 45th Rencontres de Moriond on QCD and High Energy Interactions: La Thuile, Italy, March 13-20, 2010*, pp. 135–140, Gioi Publishers, Gioi Publishers, 2010, arXiv:1006.2967.
- [28] T. Pierog *et al.*, *EPOS LHC: Test of collective hadronization with data measured at the CERN Large Hadron Collider*, Phys. Rev. C **92** (2015) 034906, arXiv:1306.0121.
- [29] D. J. Lange, *The EvtGen particle decay simulation package*, Nucl. Instrum. Meth. **A462** (2001) 152.
- [30] P. Golonka and Z. Was, *PHOTOS Monte Carlo: A precision tool for QED corrections in Z and W decays*, Eur. Phys. J. **C45** (2006) 97, arXiv:hep-ph/0506026.
- [31] Geant4 collaboration, J. Allison *et al.*, *Geant4 developments and applications*, IEEE Trans. Nucl. Sci. **53** (2006) 270.
- [32] Geant4 collaboration, S. Agostinelli *et al.*, *Geant4: A simulation toolkit*, Nucl. Instrum. Meth. **A506** (2003) 250.
- [33] M. Clemencic *et al.*, *The LHCb simulation application, Gauss: Design, evolution and experience*, J. Phys. Conf. Ser. **331** (2011) 032023.

- [34] Particle Data Group, C. Patrignani *et al.*, *Review of particle physics*, Chin. Phys. **C40** (2016) 100001.
- [35] A. Powell *et al.*, *Particle identification at LHCb*, PoS **ICHEP2010** (2010) 020, LHCb-PROC-2011-008.
- [36] A. D. Bukin, *Fitting function for asymmetric peaks*, arXiv:0711.4449.
- [37] M. Pivk and F. R. Le Diberder, *sPlot: A statistical tool to unfold data distributions*, Nucl. Instrum. Meth. **A555** (2005) 356, arXiv:physics/0402083.
- [38] LHCb collaboration, R. Aaij *et al.*, *Measurements of the branching fractions of $\Lambda_c^+ \rightarrow p\pi^-\pi^+$, $\Lambda_c^+ \rightarrow pK^-K^+$, and $\Lambda_c^+ \rightarrow p\pi^-K^+$* , JHEP **03** (2018) 043, arXiv:1711.01157.
- [39] LHCb collaboration, R. Aaij *et al.*, *Precision luminosity measurements at LHCb*, JINST **9** (2014) P12005, arXiv:1410.0149.
- [40] J.-P. Lansberg and H.-S. Shao, *Towards an automated tool to evaluate the impact of the nuclear modification of the gluon density on quarkonium, D and B meson production in proton-nucleus collisions*, Eur. Phys. J. **C77** (2017) 1, arXiv:1610.05382.
- [41] H.-S. Shao, *HELAC-Onia: An automatic matrix element generator for heavy quarkonium physics*, Comput. Phys. Commun. **184** (2013) 2562, arXiv:1212.5293.
- [42] H.-S. Shao, *HELAC-Onia 2.0: An upgraded matrix-element and event generator for heavy quarkonium physics*, Comput. Phys. Commun. **198** (2016) 238, arXiv:1507.03435.
- [43] K. J. Eskola, H. Paukkunen, and C. A. Salgado, *EPS09: A New Generation of NLO and LO Nuclear Parton Distribution Functions*, JHEP **04** (2009) 065, arXiv:0902.4154.
- [44] K. Kovarik *et al.*, *nCTEQ15 - Global analysis of nuclear parton distributions with uncertainties in the CTEQ framework*, Phys. Rev. **D93** (2016) 085037, arXiv:1509.00792.

LHCb collaboration

R. Aaij²⁷, B. Adeva⁴¹, M. Adinolfi⁴⁸, C.A. Aidala⁷⁴, Z. Ajaltouni⁵, S. Akar⁵⁹, P. Albicocco¹⁸, J. Albrecht¹⁰, F. Alessio⁴², M. Alexander⁵³, A. Alfonso Alberio⁴⁰, S. Ali²⁷, G. Alkhazov³³, P. Alvarez Cartelle⁵⁵, A.A. Alves Jr⁴¹, S. Amato², S. Amerio²³, Y. Amhis⁷, L. An³, L. Anderlini¹⁷, G. Andreassi⁴³, M. Andreotti^{16,g}, J.E. Andrews⁶⁰, R.B. Appleby⁵⁶, F. Archilli²⁷, P. d'Argent¹², J. Arnau Romeu⁶, A. Artamonov³⁹, M. Artuso⁶¹, K. Arzymatov³⁷, E. Aslanides⁶, M. Atzeni⁴⁴, B. Audurier²², S. Bachmann¹², J.J. Back⁵⁰, S. Baker⁵⁵, V. Balagura^{7,b}, W. Baldini¹⁶, A. Baranov³⁷, R.J. Barlow⁵⁶, S. Barsuk⁷, W. Barter⁵⁶, F. Baryshnikov⁷⁰, V. Batozskaya³¹, B. Batsukh⁶¹, V. Battista⁴³, A. Bay⁴³, J. Beddow⁵³, F. Bedeschi²⁴, I. Bediaga¹, A. Beiter⁶¹, L.J. Bel²⁷, N. Belyi⁶³, V. Bellec⁴³, N. Belloli^{20,i}, K. Belous³⁹, I. Belyaev^{34,42}, E. Ben-Haim⁸, G. Bencivenni¹⁸, S. Benson²⁷, S. Beranek⁹, A. Berezhnoy³⁵, R. Bernet⁴⁴, D. Berninghoff¹², E. Bertholet⁸, A. Bertolin²³, C. Betancourt⁴⁴, F. Betti^{15,42}, M.O. Bettler⁴⁹, M. van Beuzekom²⁷, I.a. Bezshyiko⁴⁴, S. Bhasin⁴⁸, J. Bhom²⁹, S. Bifani⁴⁷, P. Billoir⁸, A. Birnkraut¹⁰, A. Bizzeti^{17,u}, M. Bjørn⁵⁷, M.P. Blago⁴², T. Blake⁵⁰, F. Blanc⁴³, S. Blusk⁶¹, D. Bobulska⁵³, V. Bocci²⁶, O. Boente Garcia⁴¹, T. Boettcher⁵⁸, A. Bondar^{38,w}, N. Bondar³³, S. Borghi^{56,42}, M. Borisyak³⁷, M. Borsato⁴¹, F. Bossu⁷, M. Boubdir⁹, T.J.V. Bowcock⁵⁴, C. Bozzi^{16,42}, S. Braun¹², M. Brodski⁴², J. Brodzicka²⁹, A. Brossa Gonzalo⁵⁰, D. Brundu²², E. Buchanan⁴⁸, A. Buonaura⁴⁴, C. Burr⁵⁶, A. Bursche²², J. Buytaert⁴², W. Byczynski⁴², S. Cadeddu²², H. Cai⁶⁴, R. Calabrese^{16,g}, R. Calladine⁴⁷, M. Calvi^{20,i}, M. Calvo Gomez^{40,m}, A. Camboni^{40,m}, P. Campana¹⁸, D.H. Campora Perez⁴², L. Capriotti⁵⁶, A. Carbone^{15,e}, G. Carboni²⁵, R. Cardinale^{19,h}, A. Cardini²², P. Carniti^{20,i}, L. Carson⁵², K. Carvalho Akiba², G. Casse⁵⁴, L. Cassina²⁰, M. Cattaneo⁴², G. Cavallero^{19,h}, R. Cenci^{24,p}, D. Chamont⁷, M.G. Chapman⁴⁸, M. Charles⁸, Ph. Charpentier⁴², G. Chatzikonstantinidis⁴⁷, M. Chefdeville⁴, V. Chekalina³⁷, C. Chen³, S. Chen²², S.-G. Chitic⁴², V. Chobanova⁴¹, M. Chruszcz⁴², A. Chubykin³³, P. Ciambone¹⁸, X. Cid Vidal⁴¹, G. Ciezarek⁴², P.E.L. Clarke⁵², M. Clemencic⁴², H.V. Cliff⁴⁹, J. Closier⁴², V. Coco⁴², J.A.B. Coelho⁷, J. Cogan⁶, E. Cogneras⁵, L. Cojocariu³², P. Collins⁴², T. Colombo⁴², A. Comerma-Montells¹², A. Contu²², G. Coombs⁴², S. Coquereau⁴⁰, G. Corti⁴², M. Corvo^{16,g}, C.M. Costa Sobral⁵⁰, B. Couturier⁴², G.A. Cowan⁵², D.C. Craik⁵⁸, A. Crocombe⁵⁰, M. Cruz Torres¹, R. Currie⁵², C. D'Ambrosio⁴², F. Da Cunha Marinho², C.L. Da Silva⁷⁵, E. Dall'Occo²⁷, J. Dalseno⁴⁸, A. Danilina³⁴, A. Davis³, O. De Aguiar Francisco⁴², K. De Bruyn⁴², S. De Capua⁵⁶, M. De Cian⁴³, J.M. De Miranda¹, L. De Paula², M. De Serio^{14,d}, P. De Simone¹⁸, C.T. Dean⁵³, D. Decamp⁴, L. Del Buono⁸, B. Delaney⁴⁹, H.-P. Dembinski¹¹, M. Demmer¹⁰, A. Dendek³⁰, D. Derkach³⁷, O. Deschamps⁵, F. Desse⁷, F. Dettori⁵⁴, B. Dey⁶⁵, A. Di Canto⁴², P. Di Nezza¹⁸, S. Didenko⁷⁰, H. Dijkstra⁴², F. Dordei⁴², M. Dorigo^{42,x}, A. Dosil Suárez⁴¹, L. Douglas⁵³, A. Dovbnya⁴⁵, K. Dreimanis⁵⁴, L. Dufour²⁷, G. Dujany⁸, P. Durante⁴², J.M. Durham⁷⁵, D. Dutta⁵⁶, R. Dzhelezhyan³⁹, M. Dziwiecki¹², A. Dziurda²⁹, A. Dzyuba³³, S. Easo⁵¹, U. Egede⁵⁵, V. Egorychev³⁴, S. Eidelman^{38,w}, S. Eisenhardt⁵², U. Eitschberger¹⁰, R. Ekelhof¹⁰, L. Eklund⁵³, S. Ely⁶¹, A. Ene³², S. Escher⁹, S. Esen²⁷, T. Evans⁵⁹, A. Falabella¹⁵, N. Farley⁴⁷, S. Farry⁵⁴, D. Fazzini^{20,42,i}, L. Federici²⁵, P. Fernandez Declara⁴², A. Fernandez Prieto⁴¹, F. Ferrari¹⁵, L. Ferreira Lopes⁴³, F. Ferreira Rodrigues², M. Ferro-Luzzi⁴², S. Filippov³⁶, R.A. Fini¹⁴, M. Fiorini^{16,g}, M. Firlej³⁰, C. Fitzpatrick⁴³, T. Fiutowski³⁰, F. Fleuret^{7,b}, M. Fontana^{22,42}, F. Fontanelli^{19,h}, R. Forty⁴², V. Franco Lima⁵⁴, M. Frank⁴², C. Frei⁴², J. Fu^{21,q}, W. Funk⁴², C. Färber⁴², M. Féo Pereira Rivello Carvalho²⁷, E. Gabriel⁵², A. Gallas Torreira⁴¹, D. Galli^{15,e}, S. Gallorini²³, S. Gambetta⁵², Y. Gan³, M. Gandelman², P. Gandini²¹, Y. Gao³, L.M. Garcia Martin⁷³, B. Garcia Plana⁴¹, J. García Pardiñas⁴⁴, J. Garra Tico⁴⁹, L. Garrido⁴⁰, D. Gascon⁴⁰, C. Gaspar⁴², L. Gavardi¹⁰, G. Gazzoni⁵, D. Gerick¹², E. Gersabeck⁵⁶, M. Gersabeck⁵⁶, T. Gershon⁵⁰, D. Gerstel⁶, Ph. Ghez⁴, S. Gianì⁴³, V. Gibson⁴⁹, O.G. Girard⁴³, L. Giubega³², K. Gizdov⁵², V.V. Gligorov⁸, D. Golubkov³⁴, A. Golutvin^{55,70}, A. Gomes^{1,a},

I.V. Gorelov³⁵, C. Gotti^{20,i}, E. Govorkova²⁷, J.P. Grabowski¹², R. Graciani Diaz⁴⁰,
 L.A. Granado Cardoso⁴², E. Graugés⁴⁰, E. Graverini⁴⁴, G. Graziani¹⁷, A. Grecu³², R. Greim²⁷,
 P. Griffith²², L. Grillo⁵⁶, L. Gruber⁴², B.R. Gruberg Cazon⁵⁷, O. Grünberg⁶⁷, C. Gu³,
 E. Gushchin³⁶, Yu. Guz^{39,42}, T. Gys⁴², C. Göbel⁶², T. Hadavizadeh⁵⁷, C. Hadjivasiliou⁵,
 G. Haefeli⁴³, C. Haen⁴², S.C. Haines⁴⁹, B. Hamilton⁶⁰, X. Han¹², T.H. Hancock⁵⁷,
 S. Hansmann-Menzemer¹², N. Harnew⁵⁷, S.T. Harnew⁴⁸, T. Harrison⁵⁴, C. Hasse⁴², M. Hatch⁴²,
 J. He⁶³, M. Hecker⁵⁵, K. Heinicke¹⁰, A. Heister¹⁰, K. Hennessy⁵⁴, L. Henry⁷³,
 E. van Herwijnen⁴², M. Heß⁶⁷, A. Hicheur², R. Hidalgo Charman⁵⁶, D. Hill⁵⁷, M. Hilton⁵⁶,
 P.H. Hopchev⁴³, W. Hu⁶⁵, W. Huang⁶³, Z.C. Huard⁵⁹, W. Hulsbergen²⁷, T. Humair⁵⁵,
 M. Hushchyn³⁷, D. Hutchcroft⁵⁴, D. Hynds²⁷, P. Ibis¹⁰, M. Idzik³⁰, P. Ilten⁴⁷, K. Ivshin³³,
 R. Jacobsson⁴², J. Jalocha⁵⁷, E. Jans²⁷, A. Jawahery⁶⁰, F. Jiang³, M. John⁵⁷, D. Johnson⁴²,
 C.R. Jones⁴⁹, C. Joram⁴², B. Jost⁴², N. Jurik⁵⁷, S. Kandybei⁴⁵, M. Karacson⁴², J.M. Kariuki⁴⁸,
 S. Karodia⁵³, N. Kazeev³⁷, M. Kecke¹², F. Keizer⁴⁹, M. Kelsey⁶¹, M. Kenzie⁴⁹, T. Ketel²⁸,
 E. Khairullin³⁷, B. Khanji¹², C. Khurewathanakul⁴³, K.E. Kim⁶¹, T. Kirn⁹, S. Klaver¹⁸,
 K. Klimaszewski³¹, T. Klimkovich¹¹, S. Koliiev⁴⁶, M. Kolpin¹², R. Kopecna¹², P. Koppenburg²⁷,
 I. Kostyuk²⁷, S. Kotriakhova³³, M. Kozeiha⁵, L. Kravchuk³⁶, M. Kreps⁵⁰, F. Kress⁵⁵,
 P. Krokovny^{38,w}, W. Krupa³⁰, W. Krzemien³¹, W. Kucewicz^{29,l}, M. Kucharczyk²⁹,
 V. Kudryavtsev^{38,w}, A.K. Kuonen⁴³, T. Kvaratskheliya^{34,42}, D. Lacarrere⁴², G. Lafferty⁵⁶,
 A. Lai²², D. Lancierini⁴⁴, G. Lanfranchi¹⁸, C. Langenbruch⁹, T. Latham⁵⁰, C. Lazzeroni⁴⁷,
 R. Le Gac⁶, A. Leflat³⁵, J. Lefrançois⁷, R. Lefèvre⁵, F. Lemaitre⁴², O. Leroy⁶, T. Lesiak²⁹,
 B. Leverington¹², P.-R. Li⁶³, T. Li³, Z. Li⁶¹, X. Liang⁶¹, T. Likhomanenko⁶⁹, R. Lindner⁴²,
 F. Lionetto⁴⁴, V. Lisovskyi⁷, X. Liu³, D. Loh⁵⁰, A. Loi²², I. Longstaff⁵³, J.H. Lopes²,
 G.H. Lovell⁴⁹, D. Lucchesi^{23,o}, M. Lucio Martinez⁴¹, A. Lupato²³, E. Luppi^{16,g}, O. Lupton⁴²,
 A. Lusiani²⁴, X. Lyu⁶³, F. Machefert⁷, F. Maciuc³², V. Macko⁴³, P. Mackowiak¹⁰,
 S. Maddrell-Mander⁴⁸, O. Maev^{33,42}, K. Maguire⁵⁶, D. Maisuzenko³³, M.W. Majewski³⁰,
 S. Malde⁵⁷, B. Malecki²⁹, A. Malinin⁶⁹, T. Maltsev^{38,w}, G. Manca^{22,f}, G. Mancinelli⁶,
 D. Marangotto^{21,q}, J. Maratas^{5,v}, J.F. Marchand⁴, U. Marconi¹⁵, C. Marin Benito⁷,
 M. Marinangeli⁴³, P. Marino⁴³, J. Marks¹², P.J. Marshall⁵⁴, G. Martellotti²⁶, M. Martin⁶,
 M. Martinelli⁴², D. Martinez Santos⁴¹, F. Martinez Vidal⁷³, A. Massafferri¹, M. Materok⁹,
 R. Matev⁴², A. Mathad⁵⁰, Z. Mathe⁴², C. Matteuzzi²⁰, A. Mauri⁴⁴, E. Maurice^{7,b}, B. Maurin⁴³,
 A. Mazurov⁴⁷, M. McCann^{55,42}, A. McNab⁵⁶, R. McNulty¹³, J.V. Mead⁵⁴, B. Meadows⁵⁹,
 C. Meaux⁶, F. Meier¹⁰, N. Meinert⁶⁷, D. Melnychuk³¹, M. Merk²⁷, A. Merli^{21,q}, E. Michielin²³,
 D.A. Milanese⁶⁶, E. Millard⁵⁰, M.-N. Minard⁴, L. Minzoni^{16,g}, D.S. Mitzel¹², A. Mogini⁸,
 J. Molina Rodriguez^{1,y}, T. Mombächer¹⁰, I.A. Monroy⁶⁶, S. Monteil⁵, M. Morandin²³,
 G. Morello¹⁸, M.J. Morello^{24,t}, O. Morgunova⁶⁹, J. Moron³⁰, A.B. Morris⁶, R. Mountain⁶¹,
 F. Muheim⁵², M. Mulder²⁷, C.H. Murphy⁵⁷, D. Murray⁵⁶, A. Mödden¹⁰, D. Müller⁴²,
 J. Müller¹⁰, K. Müller⁴⁴, V. Müller¹⁰, P. Naik⁴⁸, T. Nakada⁴³, R. Nandakumar⁵¹, A. Nandi⁵⁷,
 T. Nanut⁴³, I. Nasteva², M. Needham⁵², N. Neri²¹, S. Neubert¹², N. Neufeld⁴², M. Neuner¹²,
 T.D. Nguyen⁴³, C. Nguyen-Mau^{43,n}, S. Nieswand⁹, R. Niet¹⁰, N. Nikitin³⁵, A. Nogay⁶⁹,
 N.S. Nolte⁴², D.P. O'Hanlon¹⁵, A. Oblakowska-Mucha³⁰, V. Obraztsov³⁹, S. Ogilvy¹⁸,
 R. Oldeman^{22,f}, C.J.G. Onderwater⁶⁸, A. Ossowska²⁹, J.M. Otalora Goicochea², P. Owen⁴⁴,
 A. Oyanguren⁷³, P.R. Pais⁴³, T. Pajero^{24,t}, A. Palano¹⁴, M. Palutan^{18,42}, G. Panshin⁷²,
 A. Papanestis⁵¹, M. Pappagallo⁵², L.L. Pappalardo^{16,g}, W. Parker⁶⁰, C. Parkes⁵⁶,
 G. Passaleva^{17,42}, A. Pastore¹⁴, M. Patel⁵⁵, C. Patrignani^{15,e}, A. Pearce⁴², A. Pellegrino²⁷,
 G. Penso²⁶, M. Pepe Altarelli⁴², S. Perazzini⁴², D. Pereima³⁴, P. Perret⁵, L. Pescatore⁴³,
 K. Petridis⁴⁸, A. Petrolini^{19,h}, A. Petrov⁶⁹, S. Petrucci⁵², M. Petruzzo^{21,q}, B. Pietrzyk⁴,
 G. Pietrzyk⁴³, M. Pikiés²⁹, M. Pili⁵⁷, D. Pinci²⁶, J. Pinzino⁴², F. Pisani⁴², A. Piucci¹²,
 V. Placinta³², S. Playfer⁵², J. Plews⁴⁷, M. Plo Casasus⁴¹, F. Polci⁸, M. Poli Lener¹⁸,
 A. Poluektov⁵⁰, N. Polukhina^{70,c}, I. Polyakov⁶¹, E. Polycarpo², G.J. Pomery⁴⁸, S. Ponce⁴²,
 A. Popov³⁹, D. Popov^{47,11}, S. Poslavskii³⁹, C. Potterat², E. Price⁴⁸, J. Prisciandaro⁴¹,

C. Prouve⁴⁸, V. Pugatch⁴⁶, A. Puig Navarro⁴⁴, H. Pullen⁵⁷, G. Punzi^{24,p}, W. Qian⁶³, J. Qin⁶³, R. Quagliani⁸, B. Quintana⁵, B. Rachwal³⁰, J.H. Rademacker⁴⁸, M. Rama²⁴, M. Ramos Pernas⁴¹, M.S. Rangel², F. Ratnikov^{37,ab}, G. Raven²⁸, M. Ravonel Salzgeber⁴², M. Reboud⁴, F. Redi⁴³, S. Reichert¹⁰, A.C. dos Reis¹, F. Reiss⁸, C. Remon Alepuz⁷³, Z. Ren³, V. Renaudin⁷, S. Ricciardi⁵¹, S. Richards⁴⁸, K. Rinnert⁵⁴, P. Robbe⁷, A. Robert⁸, A.B. Rodrigues⁴³, E. Rodrigues⁵⁹, J.A. Rodriguez Lopez⁶⁶, M. Roehrken⁴², A. Rogozhnikov³⁷, S. Roiser⁴², A. Rollings⁵⁷, V. Romanovskiy³⁹, A. Romero Vidal⁴¹, M. Rotondo¹⁸, M.S. Rudolph⁶¹, T. Ruf⁴², J. Ruiz Vidal⁷³, J.J. Saborido Silva⁴¹, N. Sagidova³³, B. Saitta^{22,f}, V. Salustino Guimaraes⁶², C. Sanchez Gras²⁷, C. Sanchez Mayordomo⁷³, B. Sanmartin Sedes⁴¹, R. Santacesaria²⁶, C. Santamarina Rios⁴¹, M. Santimaria¹⁸, E. Santovetti^{25,j}, G. Sarpis⁵⁶, A. Sarti^{18,k}, C. Satriano^{26,s}, A. Satta²⁵, M. Saur⁶³, D. Savrina^{34,35}, S. Schael⁹, M. Schellenberg¹⁰, M. Schiller⁵³, H. Schindler⁴², M. Schmelling¹¹, T. Schmelzer¹⁰, B. Schmidt⁴², O. Schneider⁴³, A. Schopper⁴², H.F. Schreiner⁵⁹, M. Schubiger⁴³, M.H. Schune⁷, R. Schwemmer⁴², B. Sciascia¹⁸, A. Sciubba^{26,k}, A. Semennikov³⁴, E.S. Sepulveda⁸, A. Sergi^{47,42}, N. Serra⁴⁴, J. Serrano⁶, L. Sestini²³, A. Seuthe¹⁰, P. Seyfert⁴², M. Shapkin³⁹, Y. Shcheglov^{33,†}, T. Shears⁵⁴, L. Shekhtman^{38,w}, V. Shevchenko⁶⁹, E. Shmanin⁷⁰, B.G. Siddi¹⁶, R. Silva Coutinho⁴⁴, L. Silva de Oliveira², G. Simi^{23,o}, S. Simone^{14,d}, N. Skidmore¹², T. Skwarnicki⁶¹, J.G. Smeaton⁴⁹, E. Smith⁹, I.T. Smith⁵², M. Smith⁵⁵, M. Soares¹⁵, I. Soares Lavra¹, M.D. Sokoloff⁵⁹, F.J.P. Soler⁵³, B. Souza De Paula², B. Spaan¹⁰, P. Spradlin⁵³, F. Stagni⁴², M. Stahl¹², S. Stahl⁴², P. Stefko⁴³, S. Stefkova⁵⁵, O. Steinkamp⁴⁴, S. Stemmle¹², O. Stenyakin³⁹, M. Stepanova³³, H. Stevens¹⁰, S. Stone⁶¹, B. Storaci⁴⁴, S. Stracka^{24,p}, M.E. Stramaglia⁴³, M. Straticiu³², U. Straumann⁴⁴, S. Strokov⁷², J. Sun³, L. Sun⁶⁴, K. Swientek³⁰, V. Syropoulos²⁸, T. Szumlak³⁰, M. Szymanski⁶³, S. T’Jampens⁴, Z. Tang³, A. Tayduganov⁶, T. Tekampe¹⁰, G. Tellarini¹⁶, F. Teubert⁴², E. Thomas⁴², J. van Tilburg²⁷, M.J. Tilley⁵⁵, V. Tisserand⁵, M. Tobin³⁰, S. Tolk⁴², L. Tomassetti^{16,g}, D. Tonelli²⁴, D.Y. Tou⁸, R. Tourinho Jadallah Aoude¹, E. Tournefier⁴, M. Trail⁵³, M.T. Tran⁴³, A. Trisovic⁴⁹, A. Tsaregorodtsev⁶, G. Tuci²⁴, A. Tully⁴⁹, N. Tuning^{27,42}, A. Ukleja³¹, A. Usachov⁷, A. Ustyuzhanin³⁷, U. Uwer¹², A. Vagner⁷², V. Vagnoni¹⁵, A. Valassi⁴², S. Valat⁴², G. Valenti¹⁵, R. Vazquez Gomez⁴², P. Vazquez Regueiro⁴¹, S. Vecchi¹⁶, M. van Veghel²⁷, J.J. Velthuis⁴⁸, M. Veltri^{17,r}, G. Veneziano⁵⁷, A. Venkateswaran⁶¹, T.A. Verlage⁹, M. Vernet⁵, M. Veronesi²⁷, N.V. Veronika¹³, M. Vesterinen⁵⁷, J.V. Viana Barbosa⁴², D. Vieira⁶³, M. Vieites Diaz⁴¹, H. Viemann⁶⁷, X. Vilasis-Cardona^{40,m}, A. Vitkovskiy²⁷, M. Vitti⁴⁹, V. Volkov³⁵, A. Vollhardt⁴⁴, B. Voneki⁴², A. Vorobyev³³, V. Vorobyev^{38,w}, J.A. de Vries²⁷, C. Vázquez Sierra²⁷, R. Waldi⁶⁷, J. Walsh²⁴, J. Wang⁶¹, M. Wang³, Y. Wang⁶⁵, Z. Wang⁴⁴, D.R. Ward⁴⁹, H.M. Wark⁵⁴, N.K. Watson⁴⁷, D. Websdale⁵⁵, A. Weiden⁴⁴, C. Weisser⁵⁸, M. Whitehead⁹, J. Wicht⁵⁰, G. Wilkinson⁵⁷, M. Wilkinson⁶¹, I. Williams⁴⁹, M.R.J. Williams⁵⁶, M. Williams⁵⁸, T. Williams⁴⁷, F.F. Wilson^{51,42}, J. Wimberley⁶⁰, M. Winn⁷, J. Wishahi¹⁰, W. Wislicki³¹, M. Witek²⁹, G. Wormser⁷, S.A. Wotton⁴⁹, K. Wyllie⁴², D. Xiao⁶⁵, Y. Xie⁶⁵, A. Xu³, M. Xu⁶⁵, Q. Xu⁶³, Z. Xu³, Z. Xu⁴, Z. Yang³, Z. Yang⁶⁰, Y. Yao⁶¹, L.E. Yeomans⁵⁴, H. Yin⁶⁵, J. Yu^{65,aa}, X. Yuan⁶¹, O. Yushchenko³⁹, K.A. Zarebski⁴⁷, M. Zavertyaev^{11,c}, D. Zhang⁶⁵, L. Zhang³, W.C. Zhang^{3,z}, Y. Zhang⁷, A. Zhelezov¹², Y. Zheng⁶³, X. Zhu³, V. Zhukov^{9,35}, J.B. Zonneveld⁵², S. Zucchelli¹⁵.

¹ Centro Brasileiro de Pesquisas Físicas (CBPF), Rio de Janeiro, Brazil

² Universidade Federal do Rio de Janeiro (UFRJ), Rio de Janeiro, Brazil

³ Center for High Energy Physics, Tsinghua University, Beijing, China

⁴ Univ. Grenoble Alpes, Univ. Savoie Mont Blanc, CNRS, IN2P3-LAPP, Annecy, France

⁵ Clermont Université, Université Blaise Pascal, CNRS/IN2P3, LPC, Clermont-Ferrand, France

⁶ Aix Marseille Univ, CNRS/IN2P3, CPPM, Marseille, France

⁷ LAL, Univ. Paris-Sud, CNRS/IN2P3, Université Paris-Saclay, Orsay, France

⁸ LPNHE, Sorbonne Université, Paris Diderot Sorbonne Paris Cité, CNRS/IN2P3, Paris, France

- ⁹*I. Physikalisches Institut, RWTH Aachen University, Aachen, Germany*
- ¹⁰*Fakultät Physik, Technische Universität Dortmund, Dortmund, Germany*
- ¹¹*Max-Planck-Institut für Kernphysik (MPIK), Heidelberg, Germany*
- ¹²*Physikalisches Institut, Ruprecht-Karls-Universität Heidelberg, Heidelberg, Germany*
- ¹³*School of Physics, University College Dublin, Dublin, Ireland*
- ¹⁴*INFN Sezione di Bari, Bari, Italy*
- ¹⁵*INFN Sezione di Bologna, Bologna, Italy*
- ¹⁶*INFN Sezione di Ferrara, Ferrara, Italy*
- ¹⁷*INFN Sezione di Firenze, Firenze, Italy*
- ¹⁸*INFN Laboratori Nazionali di Frascati, Frascati, Italy*
- ¹⁹*INFN Sezione di Genova, Genova, Italy*
- ²⁰*INFN Sezione di Milano-Bicocca, Milano, Italy*
- ²¹*INFN Sezione di Milano, Milano, Italy*
- ²²*INFN Sezione di Cagliari, Monserrato, Italy*
- ²³*INFN Sezione di Padova, Padova, Italy*
- ²⁴*INFN Sezione di Pisa, Pisa, Italy*
- ²⁵*INFN Sezione di Roma Tor Vergata, Roma, Italy*
- ²⁶*INFN Sezione di Roma La Sapienza, Roma, Italy*
- ²⁷*Nikhef National Institute for Subatomic Physics, Amsterdam, Netherlands*
- ²⁸*Nikhef National Institute for Subatomic Physics and VU University Amsterdam, Amsterdam, Netherlands*
- ²⁹*Henryk Niewodniczanski Institute of Nuclear Physics Polish Academy of Sciences, Kraków, Poland*
- ³⁰*AGH - University of Science and Technology, Faculty of Physics and Applied Computer Science, Kraków, Poland*
- ³¹*National Center for Nuclear Research (NCBJ), Warsaw, Poland*
- ³²*Horia Hulubei National Institute of Physics and Nuclear Engineering, Bucharest-Magurele, Romania*
- ³³*Petersburg Nuclear Physics Institute (PNPI), Gatchina, Russia*
- ³⁴*Institute of Theoretical and Experimental Physics (ITEP), Moscow, Russia*
- ³⁵*Institute of Nuclear Physics, Moscow State University (SINP MSU), Moscow, Russia*
- ³⁶*Institute for Nuclear Research of the Russian Academy of Sciences (INR RAS), Moscow, Russia*
- ³⁷*Yandex School of Data Analysis, Moscow, Russia*
- ³⁸*Budker Institute of Nuclear Physics (SB RAS), Novosibirsk, Russia*
- ³⁹*Institute for High Energy Physics (IHEP), Protvino, Russia*
- ⁴⁰*ICCUB, Universitat de Barcelona, Barcelona, Spain*
- ⁴¹*Instituto Galego de Física de Altas Enerxías (IGFAE), Universidade de Santiago de Compostela, Santiago de Compostela, Spain*
- ⁴²*European Organization for Nuclear Research (CERN), Geneva, Switzerland*
- ⁴³*Institute of Physics, Ecole Polytechnique Fédérale de Lausanne (EPFL), Lausanne, Switzerland*
- ⁴⁴*Physik-Institut, Universität Zürich, Zürich, Switzerland*
- ⁴⁵*NSC Kharkiv Institute of Physics and Technology (NSC KIPT), Kharkiv, Ukraine*
- ⁴⁶*Institute for Nuclear Research of the National Academy of Sciences (KINR), Kyiv, Ukraine*
- ⁴⁷*University of Birmingham, Birmingham, United Kingdom*
- ⁴⁸*H.H. Wills Physics Laboratory, University of Bristol, Bristol, United Kingdom*
- ⁴⁹*Cavendish Laboratory, University of Cambridge, Cambridge, United Kingdom*
- ⁵⁰*Department of Physics, University of Warwick, Coventry, United Kingdom*
- ⁵¹*STFC Rutherford Appleton Laboratory, Didcot, United Kingdom*
- ⁵²*School of Physics and Astronomy, University of Edinburgh, Edinburgh, United Kingdom*
- ⁵³*School of Physics and Astronomy, University of Glasgow, Glasgow, United Kingdom*
- ⁵⁴*Oliver Lodge Laboratory, University of Liverpool, Liverpool, United Kingdom*
- ⁵⁵*Imperial College London, London, United Kingdom*
- ⁵⁶*School of Physics and Astronomy, University of Manchester, Manchester, United Kingdom*
- ⁵⁷*Department of Physics, University of Oxford, Oxford, United Kingdom*
- ⁵⁸*Massachusetts Institute of Technology, Cambridge, MA, United States*
- ⁵⁹*University of Cincinnati, Cincinnati, OH, United States*
- ⁶⁰*University of Maryland, College Park, MD, United States*
- ⁶¹*Syracuse University, Syracuse, NY, United States*

- ⁶² Pontifícia Universidade Católica do Rio de Janeiro (PUC-Rio), Rio de Janeiro, Brazil, associated to ²
- ⁶³ University of Chinese Academy of Sciences, Beijing, China, associated to ³
- ⁶⁴ School of Physics and Technology, Wuhan University, Wuhan, China, associated to ³
- ⁶⁵ Institute of Particle Physics, Central China Normal University, Wuhan, Hubei, China, associated to ³
- ⁶⁶ Departamento de Física, Universidad Nacional de Colombia, Bogota, Colombia, associated to ⁸
- ⁶⁷ Institut für Physik, Universität Rostock, Rostock, Germany, associated to ¹²
- ⁶⁸ Van Swinderen Institute, University of Groningen, Groningen, Netherlands, associated to ²⁷
- ⁶⁹ National Research Centre Kurchatov Institute, Moscow, Russia, associated to ³⁴
- ⁷⁰ National University of Science and Technology "MISIS", Moscow, Russia, associated to ³⁴
- ⁷¹ National Research University Higher School of Economics, Moscow, Russia, Moscow, Russia
- ⁷² National Research Tomsk Polytechnic University, Tomsk, Russia, associated to ³⁴
- ⁷³ Instituto de Física Corpuscular, Centro Mixto Universidad de Valencia - CSIC, Valencia, Spain, associated to ⁴⁰
- ⁷⁴ University of Michigan, Ann Arbor, United States, associated to ⁶¹
- ⁷⁵ Los Alamos National Laboratory (LANL), Los Alamos, United States, associated to ⁶¹

- ^a Universidade Federal do Triângulo Mineiro (UFTM), Uberaba-MG, Brazil
- ^b Laboratoire Leprince-Ringuet, Palaiseau, France
- ^c P.N. Lebedev Physical Institute, Russian Academy of Science (LPI RAS), Moscow, Russia
- ^d Università di Bari, Bari, Italy
- ^e Università di Bologna, Bologna, Italy
- ^f Università di Cagliari, Cagliari, Italy
- ^g Università di Ferrara, Ferrara, Italy
- ^h Università di Genova, Genova, Italy
- ⁱ Università di Milano Bicocca, Milano, Italy
- ^j Università di Roma Tor Vergata, Roma, Italy
- ^k Università di Roma La Sapienza, Roma, Italy
- ^l AGH - University of Science and Technology, Faculty of Computer Science, Electronics and Telecommunications, Kraków, Poland
- ^m LIFAELS, La Salle, Universitat Ramon Llull, Barcelona, Spain
- ⁿ Hanoi University of Science, Hanoi, Vietnam
- ^o Università di Padova, Padova, Italy
- ^p Università di Pisa, Pisa, Italy
- ^q Università degli Studi di Milano, Milano, Italy
- ^r Università di Urbino, Urbino, Italy
- ^s Università della Basilicata, Potenza, Italy
- ^t Scuola Normale Superiore, Pisa, Italy
- ^u Università di Modena e Reggio Emilia, Modena, Italy
- ^v MSU - Iligan Institute of Technology (MSU-IIT), Iligan, Philippines
- ^w Novosibirsk State University, Novosibirsk, Russia
- ^x Sezione INFN di Trieste, Trieste, Italy
- ^y Escuela Agrícola Panamericana, San Antonio de Oriente, Honduras
- ^z School of Physics and Information Technology, Shaanxi Normal University (SNNU), Xi'an, China
- ^{aa} Physics and Micro Electronic College, Hunan University, Changsha City, China
- ^{ab} National Research University Higher School of Economics, Moscow, Russia

† Deceased